THE ASTRONOMICAL JOURNAL, 116:85–101, 1998 July

THE AGES OF DISTURBED FIELD ELLIPTICAL GALAXIES. I. GLOBAL PROPERTIES

DAVID R. SILVA[1]
European Southern Observatory, Karl-Schwarzschild-Strasse 2, D-85748 Garching, Germany; dsilva@eso.org

AND

GREGORY D. BOTHUN[1]
Department of Physics, University of Oregon, 120 Willamette Hall, Eugene, OR 97403; nuts@moo.uoregon.edu
Received 1997 May 21; revised 1998 February 17

ABSTRACT

Near-infrared images of elliptical galaxies with morphological signatures of recent merger activity have been obtained. If this merger activity stimulated significant and distributed star formation within the region defined by $R < 1.5R_e$, then JHK photometry in this region should detect the presence of an intermediate-age stellar population associated with this event. Our observations, however, show that these galaxies occupy the same locus of points in the $J-H$ versus $H-K$ plane as elliptical galaxies with no signs of recent merger activity. This strongly constrains the global fractional amount of intermediate-age (1–3 Gyr) stellar mass to be no more than 10%–15%, and in most cases the data are consistent with all the stellar mass being old ($T > 10$ Gyr) and metal-rich ([Fe/H] ≥ -0.3). We argue that any recent merger activity was, therefore, not accompanied by a significant episode of distributed star formation within the region defined by $R < 1.5R_e$ and that the bluer UBV colors often observed in this region for some of these galaxies are due to the accretion of lower mass companions or relative abundance differences. The possibility of a strongly centralized starburst resulting from the merger, instead of a more distributed star-forming episode, is fully discussed in Paper II of this series, in which similar tight constraints on this activity will be discussed.

Key words: galaxies: elliptical and lenticular, cD — galaxies: evolution — galaxies: formation — galaxies: stellar content — galaxies: structure

1. INTRODUCTION

It is now generally accepted that many current-epoch elliptical galaxies in low-density environments (so-called field ellipticals) have undergone at least one merger event in the last 5 Gyr. The observational evidence for these mergers includes the presence of morphological fine structure (e.g., ripples, shells, boxy isophotes) in perhaps 75% of all field elliptical galaxies (Bender et al. 1989; Schweizer & Seitzer 1992), kinematically distinct cores in $\sim$30% of elliptical galaxies (Illingworth & Franx 1989), and kinematically unsettled dust in the cores of 60%–80% of all elliptical galaxies (van Dokkum & Franx 1995). These features can persist only for 1–3 Gyr before becoming phase-mixed with the rest of the galaxy, implying relatively recent mergers (e.g., Quinn 1984; Hernquist & Quinn 1988, 1989; Barnes 1992).

It has also been shown that field elliptical galaxies with morphological fine structure tend to have stronger central Hβ absorption (Schweizer et al. 1990) and bluer integrated UBV colors within their effective radii (Schweizer & Seitzer 1992, hereafter SS92) than elliptical galaxies with little or no morphological fine structure. SS92 argued that both observations could be explained if these elliptical galaxies had been formed by major disk-disk mergers, roughly 3–5 Gyr ago, which resulted in a distributed burst of star formation. In this scenario, the strong Hβ and blue UBV colors are produced by the fading stellar population created by the merger-driven star formation event. A current manifestation of this scenario may be provided by NGC 3310. Although morphologically peculiar, NGC 3310 exhibits a surface brightness profile that is well fitted by an $r^{1/4}$ law. Furthermore, its high surface brightness, very blue colors, and copious near-UV emission (see Smith et al. 1996) suggest that NGC 3310 is currently undergoing a merger-driven burst of star formation that is distributed globally. A few gigayears from now, NGC 3310 should still bear the signature of this event in its UBV colors and Balmer absorption lines.

Consistent with the strong Hβ observed by Schweizer & Seitzer (1992), evidence for a significant variation in the luminosity-weighted mean age of the central stellar population among field elliptical galaxies has been presented by González (1993). In that study, field ellipticals were found to have a narrow range of central Mg_2 and Fe line strengths but a large range in central Hβ strength. This result is somewhat independent of global morphological fine structure. González used the Worthey (1994) evolutionary population synthesis models to argue that this range in Hβ strength represented a range in mean stellar age. González concluded that the strong central Hβ galaxies are produced by stellar populations with mean ages of 3 Gyr and younger (see also Bressan, Chiosi, & Tantalo 1996). Spectroscopically, NGC 221 (= M32) is the prototypical example of this class. However, since M32 is unlikely to be a merger remnant, it provides clear evidence that other astrophysical processes besides merging could be producing strong central Hβ strengths.

If the observed blue optical light is coming from an intermediate-age stellar population formed 2–3 Gyr ago as suggested by SS92, then this stellar population should also include many cool asymptotic giant branch (AGB) stars above the tip of the first-ascent giant branch (FGB), as do intermediate-age Magellanic Cloud clusters (Persson et al.

[1] Visiting Astronomer, Kitt Peak National Observatory, National Optical Astonromy Obervatories, operated by the Association of Universities for Research in Astronomy, Inc., under cooperative agreement with the National Science Foundation.

1983; Frogel, Mould, & Blanco 1990). As Persson et al. demonstrated, stellar populations containing a significant fraction of such intermediate-age AGB stars have distinctive near-IR colors. In particular, their $H-K$ color is quite red for their $J-H$ color relative to clusters without such stars. Thus, elliptical galaxies that have a significant contribution of their light from a population as young as 1–3 Gyr should have noticeably redder global $H-K$ colors than do galaxies with a significantly older mean age. Likewise, elliptical galaxies that contain a centrally concentrated intermediate-age (1–3 Gyr) stellar population should have very red central $H-K$ colors relative to the colors of their noncentral regions. This procedure to determine mean stellar ages has also been applied to S0 galaxies by Bothun & Gregg (1990), who found that some S0's have disks that are significantly younger than their bulge component.

To therefore provide additional constraints on the amount of intermediate-age stars in morphologically disturbed elliptical galaxies, we have obtained *JHK* images of a large sample of elliptical galaxies that exhibit a range of morphological fine structure. Our sample is principally drawn from Schweizer et al. (1990), SS92, and González (1993) and concentrates on so-called field ellipticals. It includes galaxies considered to contain "young" stellar populations based on their global optical colors (SS92) and/or central Hβ strengths (Schweizer et al. 1990; González 1993). In broad terms, our analysis uses $J-K$ as a metallicity indicator, while $H-K$ relative to $J-H$ is used to constrain the existence of cool, intermediate-age AGB stars (see also Persson et al. 1983).

We focus on the global near-IR colors of our sample galaxies in this paper. General sample properties, data acquisition and processing, and photometric calibration are discussed in § 2. The global colors of our sample galaxies and our basic observational results are presented in § 3. In § 4, our adopted framework for interpreting the near-IR colors of elliptical galaxies is discussed. Estimates for the fractional amount of intermediate-age stellar mass in our sample galaxies are presented and discussed in § 5. We discuss possible metallicity-driven origins for the excess blue light found in many of our galaxies in § 6. A general summary is presented in § 7. In a companion paper (Silva & Bothun 1998, hereafter Paper II), we discuss the central near-IR colors of our sample galaxies and how the combination of global and nuclear near-IR colors provide further clues about the formation and evolution of elliptical galaxies.

2. OBSERVATIONS

2.1. *Galaxy Sample and Basic Data*

The galaxies discussed in this paper and their basic properties are presented in Table 1. These galaxies were mostly selected from SS92 and span a range of morphological "fine structure" and "heuristic merger age" as defined by SS92. Galaxies have been separated into elliptical ($N = 22$), S0 ($N = 10$), and merger ($N = 1$) subgroups based on their gross Revised Shapley-Ames (RSA) morphological classification (Sandage & Tammann 1981). Galaxies with the global photometric signature of a "hot" stellar component (i.e., blue *UBV* colors; SS92) are indicated by a "G" in column (9) of Table 1. These galaxies are broken down into four subgroups, based on the classification of SS92: (1) G_1 refers to a possible recent (1–3 Gyr) disk-disk merger product with significant merger-driven star formation; (2) G_2 refers to a possible older (~ 5 Gyr) disk-disk merger product with significant merger-driven star formation; (3) G_T refers to possible sites of star formation events induced by gas transfer only; and (4) G_0 refers to galaxies with globally blue colors but conflicting evidence about recent merger activity and/or the origin of the blue light. To first order, galaxies in class G_1 should have the highest probability of containing intermediate-age AGB stars. Galaxies with the central photometric signature of a "hot" stellar component (i.e., strong central Hβ absorption; Schweizer et al. 1990; González 1993) are indicated by an "Hβ" in column (9) of Table 1. Finally, the presence of a "core" or "power law" central profile as determined by *Hubble Space Telescope* (*HST*) imagery (Faber et al. 1997) is indicated in column (10).

2.2. *Data Acquisition and Reduction*

JHK images of the late-type galaxies listed in Table 1 were obtained in 1993 February with the Simultaneous Quad Infrared Imaging Device (SQIID) at the KPNO 1.3 m telescope. SQIID contained four confocal Hughes Carlsbad 256×256 PtSi Schottky barrier diode arrays. While these arrays had few bad pixels, low dark current, and low read noise, they also had low quantum efficiency. In principle, simultaneous acquisition of *J*-, *H*-, *K*-, and *L*-band images was possible with SQIID. In practice, only *JHK* images were acquired during the duration of this project. Each channel had a slightly different plate scale that was $\approx 1\farcs3$ pixel^{-1}, providing an almost $5\farcm5 \times 5\farcm5$ field of view. Further details about SQIID may be found in Ellis et al. (1993).

All galaxy observations were acquired by integrating repeatedly for equal amounts of time on the object and on a nearby sky field. The centers of the sky fields were at least 7′ away at an absolute position angle of 45°. Both object and reference sky images were randomly dithered by 10″–30″ to facilitate the later removal of array defects, stars, and cosmic rays. This dithering technique also minimizes residual flat-fielding errors. The individual object/background integration times were 120 s in all filters. The exposure times were chosen as a compromise between keeping the peak counts in the galaxy plus background within the linearity range of the detectors, getting the background counts high enough so that the image noise was background limited, and sampling the temporal variation of the background adequately. In regard to the latter criteria, data were not acquired if the background was varying by more than $\approx 1\%$ over several observing cycles. The object/background cycle was repeated between five and seven times for each galaxy. Thus, total on-object integration times were typically 10–15 minutes.

Each galaxy data set was processed independently of the other galaxies observed. To process the data, a nightly dark frame was first subtracted from every object and sky image in a given data set. The nightly dark frame was constructed from the median of 31 dark exposures taken at the beginning or end of the night. No significant difference was seen between dark frames taken at the beginning and end of the night. In practice, the dark current was insignificant relative to the IR background observed in each of the bands. A nightly flat field was constructed by normalizing all the sky images taken on a given night to their median sky value and then median-combining the normalized sky images. This flat-field image was normalized to unity and divided into

TABLE 1

OBSERVATIONAL SAMPLE

NGC (1)	Σ (2)	Class (RSA) (3)	$-M_B$ (mag) (4)	A_B (mag) (5)	V_R (km s^{-1}) (6)	log D_N (7)	σ (km s^{-1}) (8)	Hot Population? (9)	Core (10)
Elliptical galaxies:									
547	...	E1	...	0.12	5524	0.59	171	...	...
596	4.60	E0	21.25	0.12	1817	0.93	151	G_T, Hβ	P
636	1.48	E1	20.76	0.10	1805	0.83	156	G_2, Hβ	...
821	...	E6	...	0.16	1716	0.86	199	...	...
1453.....	1.48	E2	22.26	0.24	3906	0.78	290	...	...
1700.....	3.70	E3	22.50	0.12	3881	0.90	233	G_2, Hβ	P
2974.....	0.00	E4	20.88	0.11	1924	0.95	222	...	...
3156.....	1.70	E5:	18.82	0.04	1296	0.68	112	G_0, Hβ	...
3193.....	0.00	E2	20.13	0.08	1378	0.93	205	...	...
3377.....	1.48	E6	19.66	0.06	689	1.06	131	G_0, Hβ	P
3379.....	0.00	E0	20.44	0.05	922	1.24	201	...	C
3605.....	2.70	E5	18.48	0.00	686	0.57	120	Hβ	P
3608.....	0.00	E1	19.87	0.00	1197	0.89	204	...	C
3610.....	7.60	E5	21.37	0.00	1765	1.02	159	G_1, Hβ	...
3640.....	6.85	E2	21.01	0.10	1302	1.03	176	G_T, Hβ	...
4125.....	6.00	E6	22.28	0.04	1340	1.11	229	G_1, Hβ	...
4168.....	3.00	E2	19.63	0.04	2307	0.74	182	...	C
4660.....	0.00	E5	19.59	0.00	1115	0.91	198	...	...
4697.....	0.00	E6	21.76	0.04	1210	1.22	165	G_0	P
4915.....	5.48	E0	21.11	0.04	3152	0.76	209	G_1, Hβ	...
5322.....	2.00	E4	22.14	0.00	1804	1.06	224	G_2, Hβ	...
5831.....	3.60	E4	20.28	0.14	1683	0.77	166	Hβ	...
S0 galaxies:									
315	...	EL	...	0.26	4956	0.82	352	...	...
584	2.78	$S0_1$(3, 5)	21.76	0.12	1875	1.06	217	Hβ	...
1023.....	...	$SB0_1$(5)	21.17	0.25	661	...	...	...	P
1052.....	1.78	E3/S0	20.89	0.06	1475	1.00	206	...	...
1172.....	...	$S0_1$(0, 3)	19.48	0.10	1669	0.58	121	...	P
2549.....	0.00	$S0_{1,2}$(7)	19.80	0.12	1082	...	...	...	...
2685.....	2.48	$S0_3$(7) pec	19.55	0.15	881	...	...	...	...
2768.....	0.00	$S0_{1,2}$(6)	21.55	0.02	1363	1.03	198	...	...
3489.....	0.00	$S0_3$/Sa	19.13	0.02	659	...	...	...	...
3607.....	0.00	$S0_3$(3)	20.71	0.00	951	1.10	248	...	...
Ongoing merger:									
3921.....	8.84	Merger	...	0.00	5926	...	...	...	...

NOTES.—Col. (1): NGC number. Col. (2): Morphological fine-structure parameter from SS92. Col. (3): Morphological classification from Revised Shapley-Ames Catalog (RSA; Sandage & Tammann 1981). Col. (4): Absolute B magnitude, from RSA. Col. (5): Foreground Galactic absorption from Burstein et al. 1987 or Burstein & Heiles 1984. Col. (6): Heliocentric radial velocity, from Burstein et al. 1987. Col. (7): log D_N from Burstein et al. 1987. Col. (8): Adopted central velocity dispersion from Davies et al. 1987. Col. (9): "Hot" population indicators: Hβ = strong central Hβ absorption (Schweizer et al. 1990 or González 1993) and G = global UBV color excess indicated by SS92. Based on discussion in SS92, galaxies are classified as follows: G_1 = possible recent (1–3 Gyr) disk-disk merger product with significant merger-driven star formation; G_2 = possible older ($\sim$5 Gyr) disk-disk merger product with significant merger-driven star formation; G_T = possible sites of recent (1–3 Gyr) star formation events induced by gas transfer only; G_0 = globally blue UBV colors but conflicting evidence about recent merger activity and/or the origin of the blue light. See SS92 for further details. Col. (10): Core morphology as defined by Faber et al. 1997 based on *HST* observations. C = core, P = power law.

each dark-subtracted object and sky image. A reference background image for each object image was then constructed by averaging the preceding and following sky images. The subtraction of this reference from the corresponding object image removes both the IR background and any residual dark current. Only one sky image was used as the reference image for the first and last object images in a given series of observations. The rms residual sky variation within a given set of frames was typically 1–2 ADU (0.1% of the background) in J, 3–4 ADU (0.3%) in H, and 2–3 ADU (0.2%) in K.

To ensure photometric accuracy, all data taken with SQIID had to be corrected for nonlinearity effects. This correction was applied using a calibration function described in the SQIID user's manual (version of 1993 January 7), provided by M. Merrill of the Kitt Peak National Observatory. That function calibrates the data to an effective exposure time equal to the requested integration time plus the offset time delay (i.e., the time between the array reset and the first array read). The effective exposure time was then used for all subsequent photometric measurements.

The individual sky-subtracted object images were then spatially replicated by a factor of 2 to allow more accurate image registration. The final image scale was $\approx 0\farcs65$ pixel^{-1}. The magnified processed images were then spatially registered, and an additive constant was applied to correct the background to zero. This set of images was then combined into a final image. During the combination process, postregistered frames were compared and deviant pixels were rejected using a median percentile clipping algorithm described in the IRAF IMCOMBINE help page.[2]

[2] The Image Reduction and Analysis Facility (IRAF) is distributed by the National Optical Astronomy Observatories.

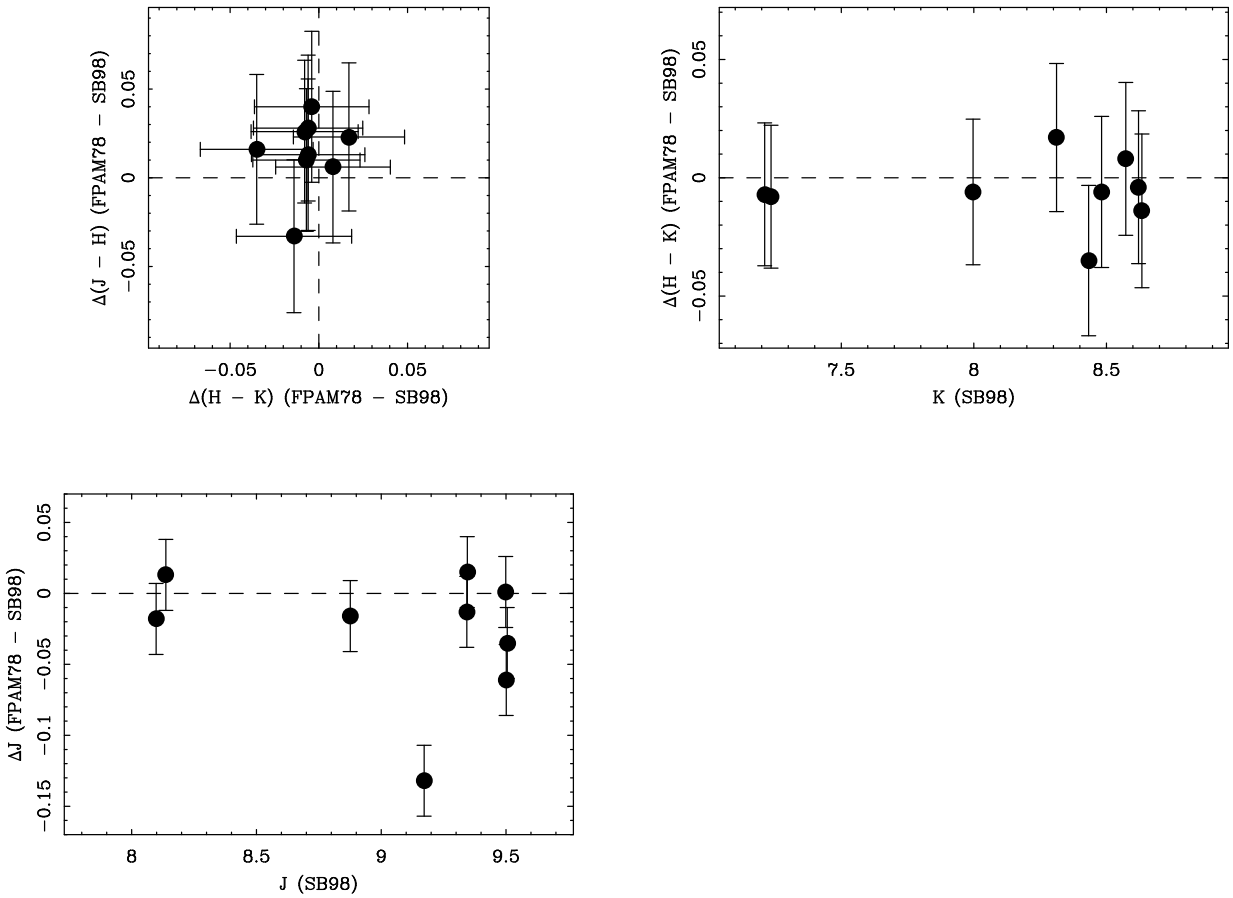

FIG. 1.—Near-IR photometric measurement differences between FRAM78 and this paper are shown for the nine galaxies these two studies have in common. All measurements are through a 48″ diameter circular aperture. The error bars drawn are the color uncertainties listed in Table 2. *Top left*, differences in the near-IR color-color plane; *top right*, color difference as a function of measured K magnitude; *bottom*, magnitude difference as a function of measured J magnitude. As the color-color panel illustrates, there is a tendency for the new measurements to be slightly redder in $J-H$, although the new and FRAM78 measurements are consistent within the current uncertainties. The other panels illustrate that while the magnitude and color difference *scatter* increases with decreasing luminosity, magnitude and color difference *magnitude* are not correlated with luminosity.

The cleaned images were then averaged. The final image was smoothed by a two-dimensional $\sigma = 0.8$ pixel Gaussian to remove artificial high-frequency information induced by replication.

The relatively large SQIID field of view of 5.′5 × 5.′5 allowed us to make an in situ background correction. For each final galaxy image, a median value was computed within a tightly windowed intensity range of typically −100 to 100 counts. This median was then subtracted from the frame. A residual background uncertainty σ_i was estimated by measuring the background in several places on the frame and then computed in standard deviation of those measurements. The typical uncertainty was ∼0.2 ADU (0.01%–0.03% of the original background; see above). This procedure may overestimate the background for the nearest galaxies in our sample, introducing a small systematic error. Consider the nearest galaxy in our sample, NGC 3379. Any systematic error introduced by our background correction will be largest for this galaxy. The actual central instrumental J intensity was ∼8200 ADU. Assume that the luminosity profile of NGC 3379 closely follows an $r^{1/4}$ law with an optical effective radius of ∼35″ (e.g., Peletier 1989). Further assume that the J-band effective radius is also 35″. On average, the residual background uncertainty for the J-band image of NGC 3379 was measured at a galactocentric radius of 150″. Given an effective radius of 35″ and a central intensity of 8200 ADU, we estimate that NGC 3379 has an instrumental J-band surface brightness of 0.13 ADU pixel^{-1} at $r = 150''$. In an aperture of diameter D_N (see Table 1), a background error of 0.13 ADU corresponds to a J-band instrumental magnitude error of 0.005 mag. For reference, a 1 ADU error would produce a 0.035 mag error; this is the worst case. Most of our other galaxies are far enough away that they produce much less light at this radius. We return to this point in § 2.4.

Instrumental aperture magnitudes were then measured for each galaxy using standard IRAF tools. From these instrumental magnitudes, we then calculated instrumental colors (e.g., $j-k$) and color uncertainties (σ_{j-k}) using sets of equations of the following form:

$$
\begin{aligned}
j-k &= -2.5 \log (f_j/f_k) , \\
j-k^+ &= -2.5 \log [(f_j + \sigma_j A_{\rm ap}/T_{\rm exp})/(f_k - \sigma_k A_{\rm ap}/T_{\rm exp})] , \\
j-k^- &= -2.5 \log [(f_j - \sigma_j A_{\rm ap}/T_{\rm exp})/(f_k + \sigma_k A_{\rm ap}/T_{\rm exp})] , \\
\sigma_{j-k} &= (j-k^+ + j-k^-)/2 , \qquad (1)
\end{aligned}
$$

where f_i is the integrated background-corrected flux in band i within some aperture in ADU s^{-1}, $A_{\rm ap}$ is the area of the aperture in pixels, σ_i is the random background uncertainty in band i in counts per pixel, and $T_{\rm exp}$ is the exposure time. These errors are random errors and do not include any

systematic background errors or any transformation uncertainties.

This process was repeated for each band. The actual processing was done using IRAF scripts written by one of the authors (D. R. S.).

2.3. *Photometric Calibration*

The galaxy instrumental photometry were transfered into the CIT near-IR photometric system using observations of the Elias et al. (1983) faint standard stars (see their Table 2). The color ranges of the observed stars were 0.00–1.03 in $J-K$ and 0.0–0.36 in $H-K$.

Each night 10–15 standard stars were observed. Each standard was observed 6 times: first in the center of the arrays, then near each of the four corners in sequence, and finally near the center again. These frames were linearized as described above for the galaxy data. The six standard-star images were combined into a "local" dark/background frame using the median percentile clipping algorithm described by Valdes (1991). After subtraction of that image, each standard image was divided by a normalized flat image constructed as described above. The instrumental magnitudes were measured and then averaged. The mean instrumental magnitude of the six standard observations was used as the assigned instrumental magnitude. The typical standard deviation of these mean instrumental magnitudes was 0.02 mag or less.

Nightly photometric transformations were derived using the IRAF PHOTCAL tool. On a photometric night, the typical rms variations about the nightly photometric transformations were 0.01 mag or less for all three bands. The following mean photometric transformations were adopted:

$$\begin{aligned} J &= j + \zeta_J - 0.14\chi_J - 0.04(J-K)\,, \\ H &= h + \zeta_H - 0.06\chi_H - 0.18(H-K)\,, \\ K &= k + \zeta_K - 0.09\chi_K - 0.02(J-K)\,, \end{aligned} \tag{2}$$

where j, h, and k are the instrumental magnitudes, ζ_j, ζ_h, and ζ_k are the zero points determined nightly, and χ_J, χ_H, and χ_K are the air masses at which objects were observed in the indicated photometric bands.

2.4. *Comparison with Frogel et al. (1978)*

The use of Elias et al. (1983) standards places our data in the near-IR CIT photometric system, the same system used by Frogel et al. (1978, hereafter FPAM78). In Figure 1, the residuals between our color measurements and the FPAM78 color measurements through 48″ diameter circular apertures are shown for all galaxies common between these two samples. In general, the agreement is good and within the reported FPAM78 errors. We conclude that we can directly compare our photometry with the previously published FPAM78 photometry without any further transformations.

Figure 1 also demonstrates that any systematic error introduced by our residual background correction procedure must be small within this 48″ diameter aperture. If it were significant, the brighter galaxies would have larger deviations from the FPAM78 data than the fainter galaxies, which is clearly not the case.

3. OBSERVATIONAL RESULTS

The main observational goals of this study were to measure the central and global colors of our sample of elliptical galaxies. We chose to make these measurements using both circular and elliptical apertures. Circular aperture photometry is useful because it can be easily compared with previously published photometric studies. Furthermore, there is no geometric ambiguity about circular apertures: they are only defined by their center and radius. Elliptical apertures, on the other hand, have the advantage of conforming more closely to the shape of each galaxy and how that shape changes with increasing semimajor axis: they will measure more accurately the colors of geometric dependent features (e.g., central, flattened disks). Presumably, it is these features that also help determine the morphological fine structure. In this paper, we discuss only circular aperture photometry, and only in the context of global colors. We discuss the methodology of our elliptical aperture photometry and the central colors of our galaxies in Paper II.

The chief observational result of SS92 was that galaxies with morphological fine structure exhibited UBV colors measured within their effective radii apertures that were significantly bluer than other elliptical galaxies of similar M_B measured through their effective radii aperture. They argued that the "blue" elliptical galaxies with the most disturbed morphologies had been formed within the last 4–7 Gyr by major disk-disk merger events that were accompanied by a major star formation episode (such as is apparently occurring now in NGC 3310), while "blue" elliptical galaxies with more normal morphologies had merely been rejuvenated by some sort of gas transfer.[3] If these galaxies do contain an intermediate-age stellar population as young as is asserted by SS92, then they should have significantly redder $H-K$ colors at a given $J-H$ color than do the undisturbed, "older" elliptical galaxies observed by SS92. In general, our integrations were long enough that accurate photometry can be obtained within (1–1.5)R_e, and hence we can search for redder $H-K$ colors in the same region in which SS92 measured their bluer UBV colors.

Choosing a meaningful aperture size is somewhat subjective. One could choose a standard metric aperture size (e.g., 2 kpc), but that implicitly assumes that all observed galaxies have the same underlying light distribution and only differ in their relative distances. Even if this were true, defining accurate metric apertures requires accurate distances, which are unavailable for most of the galaxies in our sample. We elected to measure our colors through apertures of diameter D_N taken from Burstein et al. (1987). Recall that D_N is defined to be the diameter of the circular aperture within which a galaxy has a mean predefined surface brightness. As Dressler et al. (1987) and Djorgovski & Davis (1987) demonstrated, log D_N is correlated with log σ, the central velocity dispersion and, therefore, something like total galaxy stellar mass. Thus, D_N is physically related to the intrinsic properties of each galaxy and is independent of its distance (which is, of course, why the D_N-σ relationship and

[3] Of course, if these hypotheses are correct, then it seems likely that the M_B of these "blue" elliptical galaxies is biased toward higher luminosities because of the presence of a younger, hotter stellar population than putatively quiescent elliptical galaxies of similar mass, i.e., younger elliptical galaxies should have a smaller M/L_B. Using the M_B of "blue" elliptical galaxies to predict their color based on a color-magnitude relationship dominated by "red" galaxies will naturally predict colors that are too red and therefore increase the color contrast between the "blue" and the "red" elliptical galaxies (see, e.g., Gregg 1992 and rebuttal in SS92 for further discussion of this point).

its associated fundamental-plane variants are used as distance indicators).

For all galaxies with D_N values published in Burstein et al. (1987), near-IR colors are presented in Table 2. This corresponds to 28 of the 33 galaxies listed in Table 1. The colors were measured through centered circular apertures of diameter D_N. The observed colors presented in columns (4) and (5) were transformed from the instrumental colors using equation (2) and the appropriate nightly zero point. Corresponding uncertainties, calculated as discussed in § 2.2, are presented in columns (6) and (7). The colors listed in columns (8) and (9) were corrected for Galactic reddening using the A_B values listed in Table 1 and the parameterized reddening law of Cardelli, Clayton, & Mathis (1989). These colors were also corrected for redshift using the redshifts listed in Table 1 and the K-corrections given in FPAM78.

The near-IR two-color distribution of the galaxies listed in Table 2 is shown in Figure 2. Clearly, there is no significant color separation between the "young" and "old" galaxies in Figure 2 within the observational uncertainties. Furthermore, there are no galaxies at all that have $H-K > 0.25$. Given the colors of intermediate-age Magellanic Cloud clusters, if there were galaxies in our sample that contained a significant amount of intermediate-age mass, we would have expected to detect galaxies with $H-K$ colors ranging from 0.25 to 0.45 depending on the amount of AGB mass present. To first order, this result seems rather difficult to reconcile with the notion that elliptical galaxies have a large spread in their mean stellar ages. Using data obtained for Silva & Elston (1994), we have also shown the colors for M32. Note that its global colors are very similar to the rest of the sample, even though M32 is known to contain an extended giant branch (Elston & Silva 1992; Freedman 1992). Measuring colors through apertures defined by the B-band half-light radius as listed in the RC3 (de Vaucouleurs et al. 1991) does not change our conclusions.

This general lack of color separation between putatively "young" and "old" elliptical galaxies, as well as elliptical galaxies and S0's, is also illustrated in Figure 3, in which $J-K$ is plotted against log σ, central velocity dispersion, and log D_N. These latter quantities are correlated with total mass and luminosity, respectively, and, of course, are correlated with each other via the fundamental-plane correlations. The linear relations between these pairs of parameters derived by Bower, Lucey, & Ellis (1992) for Virgo and Coma Cluster elliptical galaxies are shown as dashed lines. The zero points have been shifted to minimize the scatter of the current data set about the cluster correlations. Bower et al. found that the cluster correlations were

TABLE 2

GALAXY PHOTOMETRY

NGC (1)	σ (km s^{-1}) (2)	log D_N (3)	$J-H$ (mag) (4)	σ_{J-H} (mag) (5)	$H-K$ (mag) (6)	σ_{H-K} (mag) (7)	$(J-H)_0$ (mag) (8)	$(H-K)_0$ (mag) (9)
315	352	0.82	0.69	0.01	0.27	0.01	0.61	0.16
547	171	0.59	0.73	0.01	0.22	0.01	0.69	0.13
584	217	1.06	0.64	0.02	0.23	0.01	0.60	0.18
596	151	0.93	0.68	0.02	0.19	0.01	0.64	0.14
636	156	0.83	0.68	0.02	0.20	0.01	0.65	0.16
821	199	0.86	0.67	0.01	0.23	0.01	0.63	0.18
1052.....	206	1.00	0.70	0.01	0.22	0.01	0.68	0.19
1172.....	121	0.58	0.68	0.01	0.21	0.01	0.65	0.17
1453.....	290	0.78	0.72	0.01	0.27	0.01	0.65	0.17
1700.....	233	0.90	0.68	0.01	0.24	0.01	0.64	0.17
2768.....	198	1.03	0.67	0.01	0.21	0.01	0.66	0.19
2974.....	222	0.95	0.67	0.01	0.25	0.01	0.64	0.20
3156.....	112	0.68	0.61	0.02	0.22	0.02	0.59	0.20
3193.....	205	0.93	0.65	0.02	0.20	0.01	0.63	0.17
3377.....	131	1.06	0.65	0.02	0.19	0.01	0.63	0.17
3379.....	201	1.24	0.65	0.01	0.20	0.01	0.64	0.18
3607.....	248	1.10	0.67	0.01	0.25	0.01	0.66	0.24
3608.....	204	0.89	0.66	0.01	0.22	0.01	0.66	0.21
3610.....	159	1.02	0.65	0.02	0.22	0.01	0.65	0.20
3640.....	176	1.03	0.67	0.02	0.20	0.01	0.63	0.16
3921.....	279	0.67	0.65	0.03	0.28	0.02	0.63	0.21
4125.....	229	1.11	0.66	0.01	0.22	0.01	0.65	0.19
4168.....	182	0.74	0.66	0.01	0.20	0.01	0.64	0.16
4660.....	198	0.91	0.65	0.01	0.20	0.01	0.65	0.18
4697.....	165	1.22	0.65	0.02	0.18	0.01	0.64	0.16
4915.....	209	0.76	0.68	0.01	0.22	0.01	0.66	0.18
5322.....	224	1.06	0.67	0.01	0.19	0.01	0.66	0.17
5831.....	166	0.77	0.66	0.01	0.24	0.01	0.62	0.19

NOTES.—Col. (1): NGC number. Col. (2): Adopted central velocity dispersion from Davies et al. 1987. Col. (3): log D_N from Burstein et al. 1987 for all galaxies except NGC 3921. For the ongoing merger NGC 3921, this is the V-band effective radius of the main body (see Schweizer 1996, Table 6), in the same units as log D_N. Col. (4): Measured $J-H$, using a circular aperture of diameter log D_N. Col. (5): Uncertainty in $J-H$ (see text for details). Col. (6): Measured $H-K$ using a circular aperture of diameter log D_N. Col. (7): Uncertainty in $H-K$ (see text for details). Col. (8): $J-H$ corrected for foreground Galactic absorption and redshift (see text for details). Col. (9): $H-K$ corrected for foreground Galactic absorption and redshift (see text for details).

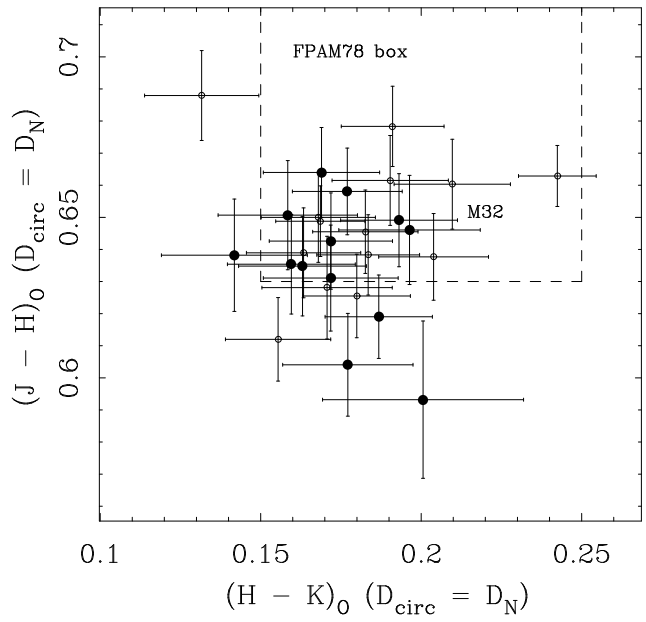

FIG. 2.—Colors measured through circular apertures with diameter D_N for all the *elliptical* galaxies in our sample. Error bars illustrate random photometric errors. The filled symbols denote galaxies that are classified as "young" by virtue of their blue optical colors and/or strong central Hβ absorption. The colors for M32 come from Silva & Elston (1994). The M32 color uncertainties are smaller than the symbol plotted. The galaxy with the bluest $J-H$ color is NGC 3156, which is known to be actively forming stars and to have a slight lower metallicity than does the rest of our sample (see Gregg 1989). The dashed box shows the color range of the entire FPAM78 sample.

somewhat statistically significant but that the rms color scatter was ~ 0.05 mag, not dissimilar from the scatter seen in Figure 3. The main point, again, is that most of the "young" and "old" galaxies are intermixed, suggesting that they have similar cool populations. The outliers seen in these figures are the same outliers seen in Figure 2.

As discussed below in § 4.1.3, $H-K$ is most sensitive to the presence of intermediate-age AGB stars. In Figure 4, we plot $H-K$ against $\log \sigma$ and $\log D_N$. The mean $H-K$ color and its standard deviation of our sample are illustrated by solid and dashed horizontal lines, respectively. Only two galaxies appear to be significantly redder than the sample mean: NGC 3607 and M32. We discuss these two galaxies further below. None of the other galaxies are significantly redder than the mean, suggesting that none of the other galaxies contains a significant amount of intermediate-age mass. We place upper limits on the amount of intermediate-age mass in § 5.

4. INTERPRETING COMPOSITE NEAR-IR COLORS

We have seen that in general the elliptical galaxies in our sample have very similar near-IR colors. What does that tell us about the mean ages of these galaxies, and, in particular, what constraints can be placed on the amount of intermediate-age mass in these galaxies? To properly address these questions, we must first understand the various factors that could complicate the the detection of cool AGB stars via near-IR photometry.

4.1. *Stellar Population Effects*

In principle, the best way to interpret the integrated light of a composite stellar population is to use stellar population synthesis models. The basic criteria of a successful stellar population synthesis model is that it reproduces the observed colors of real galaxies. In Figure 5, Bruzual & Charlot (1993) and Worthey (1994) models are compared with the observed colors of real elliptical galaxies. These models are thought to reproduce the optical colors and line indices of elliptical galaxies with high fidelity. Alas, as Figure 5 illustrates, these models do not reproduce the observed near-IR colors of elliptical galaxies very well, nor do they agree with each other. Similar discrepancies also exist in the $J-K$ versus $V-K$ plane. This may indicate that either post–main-sequence stellar evolution, particularly of mid-K and cooler FGB and AGB stars, is not being modeled properly or that the input stellar atmospheres used to calibrate the models are faulty (see the discussion in Charlot, Worthey, & Bressan 1996). Whatever the cause of these discrepancies, interpreting the absolute near-IR colors of real galaxies within the framework of these models seems suspect at present. Even differential comparisons (e.g., interpreting a change in near-IR color as a specific change in metallicity or age) seem suspect. Caution advises that we therefore use a more empirical approach to characterize the effects of metallicity and age on the integrated light of elliptical galaxies.

4.1.1. *Old Stellar Populations*

In old ($t > 5$ Gyr) stellar populations, near-IR light is dominated by stars on the first-ascent giant branch. As Aaronson et al. (1978) were the first to show using Galactic globular clusters, $J-K$ is driven by metallicity. Broadly, this color-metallicity relationship holds because near-IR colors measure mean FGB temperature. In turn, FGB temperatures are driven by envelope opacity, which is dominated by H^-. Since metals are the primary electron donors to H^-, as metallicity increases FGB envelope opacity increases, FGB effective temperatures decrease, and mean FGB colors become redder. It is commonly argued (e.g., Bothun et al. 1984; Burstein 1985) that Fe is the dominant electron donor and therefore $J-K$ color traces relative Fe abundance almost directly. However, in combination, Mg and Si contribute the same fractional amount of electrons as does Fe (Renzini 1977), which makes $J-K$ an integrated light tracer of total metallicity, not just iron, for old populations within the metallicity range $-2.2 \leq$ [Fe/H] ≤ -0.3.

Can $J-K$ be used as a metallicity indicator in elliptical galaxies? As shown in FRAM78 (see their Fig. 4), late-type galaxies have similar $J-H$ colors but redder $H-K$ colors (again, by ~ 0.05 mag) than do the most metal-rich globular clusters with reliable near-IR data at that time. However, the more complete data set of M. Malkan & M. Aaronson (1980, unpublished) of large-aperture near-IR Galactic globular cluster photometry clearly illustrates that although [Fe/H] and integrated $J-H$ and $J-K$ colors are linearly correlated for the entire Galactic globular cluster metallicity range, the $J-H/H-K$ relationship changes at [Fe/H] ~ -0.8. Below this metallicity, $H-K$ is constant and $J-H$ becomes redder with increasing metallicity. For [Fe/H] > -0.8, however, $J-H$ and $H-K$ increase with increasing metallicity. This break corresponds to the onset of M giant formation at [Fe/H] ~ -0.6 (see, e.g., Frogel, Persson, & Cohen 1983). The most natural explanation then for the redder $H-K$ colors of elliptical galaxies is a

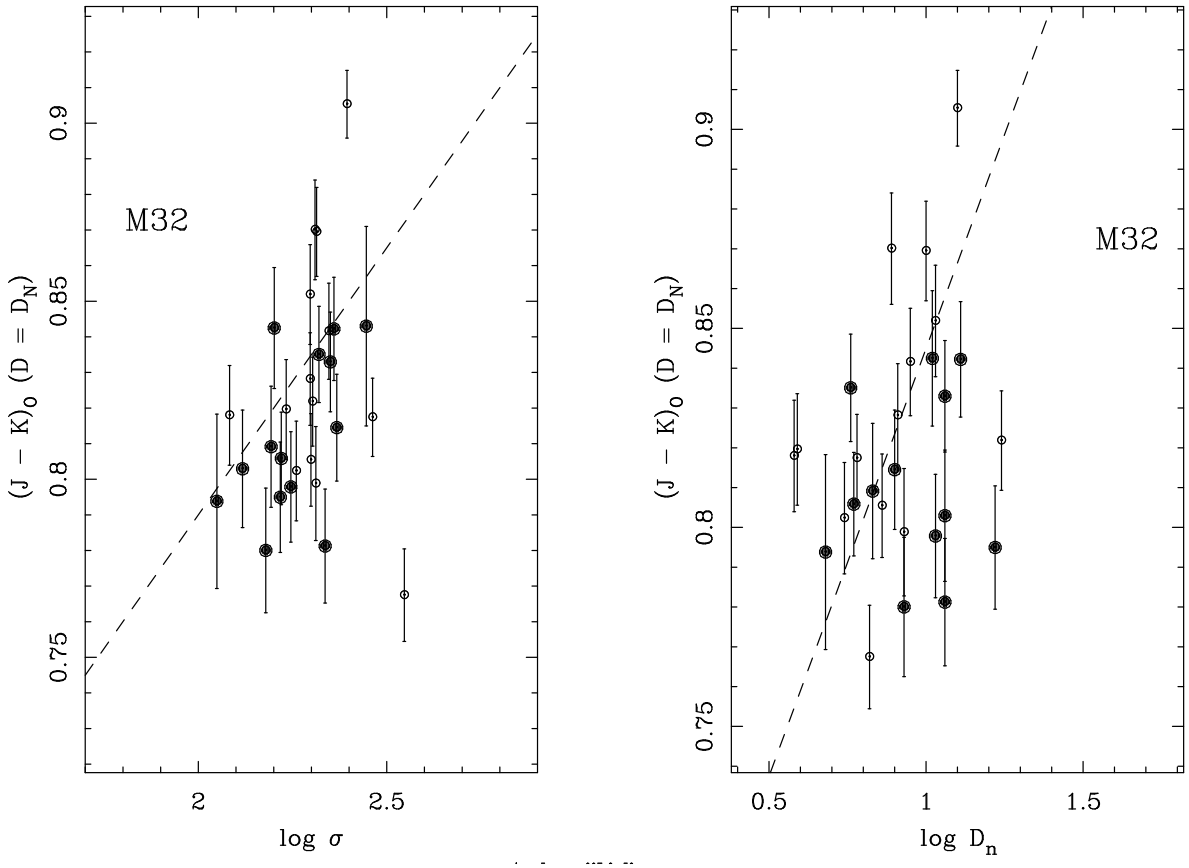

FIG. 3.—$J-K$ measured through circular apertures with diameter D_N for the *elliptical* galaxies in our sample. Colors were corrected for Galactic foreground reddening and redshift. Error bars illustrate random photometric errors. The filled symbols denote galaxies classified as "young" by virtue of their blue optical colors and/or strong central Hβ absorption. The colors for M32 come from Silva & Elston (1994). The M32 color uncertainties are smaller than the symbol plotted. The colors are plotted against central velocity dispersion (log σ) from Davies et al. (1987) and standard diameter (log D_N) from Burstein et al. (1987). The dashed lines illustrate relationships derived for Virgo and Coma Cluster elliptical galaxies by Bower et al. (1992). The zero points of these lines have been adjusted to minimize the rms scatter.

larger relative number of M giants due to their higher mean metallicity.

Furthermore, at similar [Fe/H], the M giants in elliptical galaxies may also be redder than the M giants in Galactic globular clusters due to a relative light-element abundance enhancement. Several studies have concluded that [Mg/Fe] (and perhaps the relative abundances of all light elements) is supersolar ($\approx$0.2–0.4) within elliptical galaxies (Peletier 1989; Gorgas, Efstathiou, & Salamanca 1990; Worthey, Faber, & González 1992; Davies, Sadler, & Peletier 1992). This is similar to the relative enhancement of light elements seen in Baade's window (BW) K giants, which have a mean [Fe/H] = -0.25, but enhanced Ti and Mg (by $\sim$0.3 dex) (McWilliam & Rich 1994). McWilliam & Rich argued that this is consistent with the observation that BW K giants have near-IR colors intermediate between 47 Tuc and M67, which have [Fe/H] of -0.71 and -0.09, respectively (Frogel & Whitford 1987; Davidge 1991; Tiede, Frogel, & Terndrup 1995), i.e., that $J-K$ measures the true effective temperature of these K giant stars and, therefore, their true [Fe/H]. This would explain why BW and local field K giants have the same mean near-IR colors. BW M giants, however, tend to be somewhat redder ($\sim$0.1 mag in $H-K$ for $J-H \geq 0.8$) and have stronger molecular features (e.g., TiO and CO) than do field M giants (see, e.g., Frogel & Whitford 1987; Teide et al. 1995, especially their Fig. 12).[4] If the FGB stars in luminous late-type galaxies are similar to the BW giants, it is natural that elliptical galaxies would have similar $J-H$ colors (which are dominated by K giants) but redder $H-K$ colors (which are weighted more to M giants) than metal-rich Galactic globular clusters.

How age-dependent are mean FGB temperature and, therefore, $J-H$? We can estimate the impact of age using the Revised Yale Isochrones (Green, Demarque, & King 1987). At $M_{\rm bol} = -1.5$ (which corresponds to a late K or early M star on the FGB), the typical range of log $T_{\rm eff}$ at any given Y and $0.01 \leq Z \leq 0.04$ (i.e., from half solar to twice solar metallicity) is $\sim$0.04 dex for an age range of 1–20 Gyr. But over the metallicity range $0.001 \leq Z \leq 0.04$, Δ log $T_{\rm eff} \approx 0.14$. Thus, over these entire ranges $\Delta t/\Delta Z \approx 0.33$ (cf. Worthey 1994, especially Table 6 and discussion therein).

[4] In contrast to this result, the metal-rich Galactic globular clusters Liller 1 ([Fe/H] = +0.25; Frogel, Kuchinski, & Tiede 1995) and NGC 6440 ([Fe/H] = -0.34; Kuchinski & Frogel 1995) have M giants that are redder in $J-H$ and bluer in $H-K$ than both solar-neighborhood and BW M giants, despite having [Fe/H] values that straddle the solar neighborhood and BW. How this result and the BW result are physically connected is currently unknown.

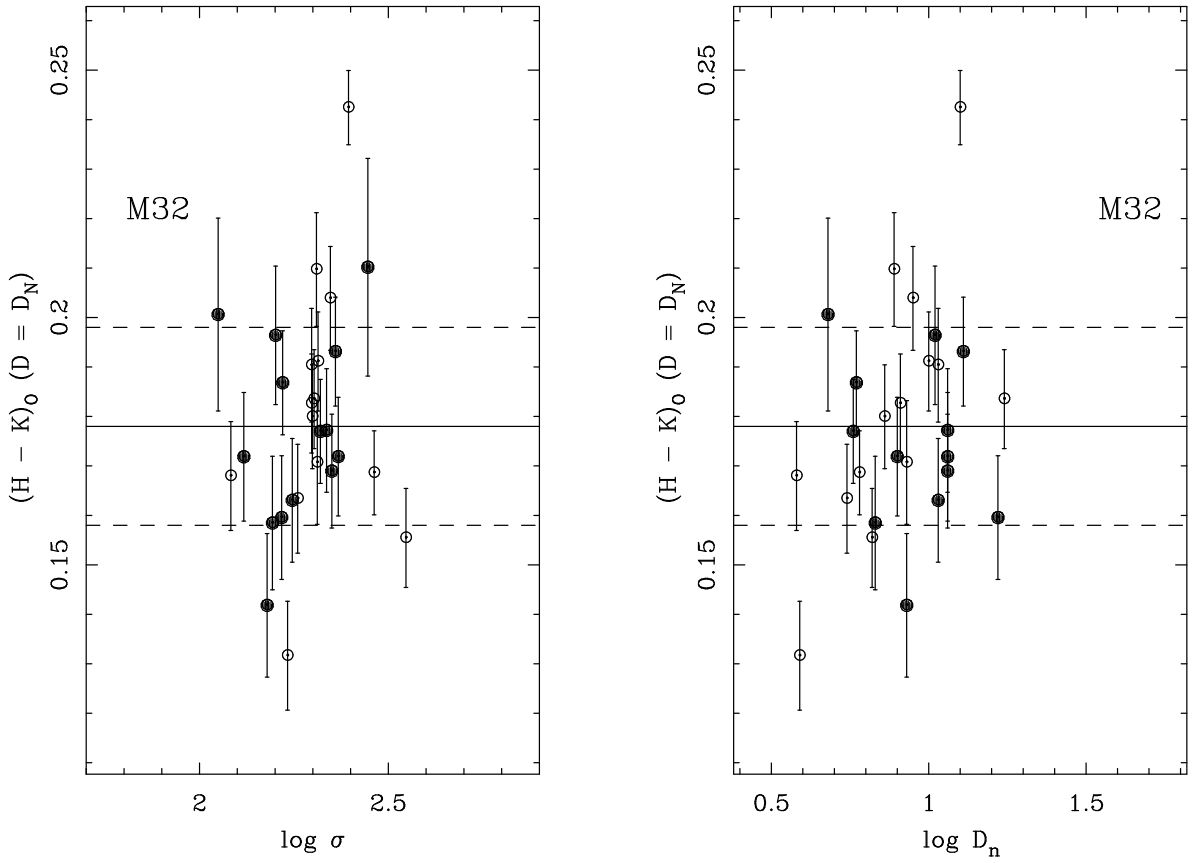

FIG. 4.—$H-K$ measured through circular apertures with diameter D_N are shown for the *elliptical* galaxies in our sample. Colors were corrected for Galactic foreground reddening and redshift. Error bars illustrate random photometric errors. The filled symbols denote galaxies that are classified as "young" by virtue of their blue optical colors and/or strong central Hβ absorption. The colors for M32 come from Silva & Elston (1994). The M32 color uncertainties are smaller than the symbol plotted. The colors are plotted against central velocity dispersion (log σ) from Davies et al. (1987) and standard diameter (log D_N) from Burstein et al. (1987). The solid line shows the weighted mean color of the galaxies shown while the dashed lines show the standard deviation of this mean. The reddest galaxy is NGC 3607; however, we conclude that its unusual color is caused by internal reddening, not the presence of an extended AGB. See text for further discussion.

However, over more restricted metallicity ($0.01 \leq Z \leq 0.04$) and age (5–10 Gyr) ranges, $\Delta t/\Delta Z < 0.25$. If we assume that $J-K$ changes linearly with $T_{\rm eff}$, then clearly $J-K$ will be much more sensitive to metallicity than to age in old, metal-rich populations. These temperature/color changes affect G/K giants primarily, and therefore $J-H$. $H-K$ is more sensitive to the temperatures of the coolest stars near and above the FGB tip, particularly M giants produced when [Fe/H] ≥ -0.8, and, therefore, is relatively insensitive to these changes in mean FGB temperature.

4.1.2. *Near-IR Metallicity Vector*

To parameterize the relationship between near-IR color and metallicity, we adopt near-IR color-metallicity relationships derived from observations of Galactic globular clusters. These relationships can be described as follows:

$$
\begin{aligned}
&J-K \propto 0.17 \pm 0.01[\mathrm{Fe/H}]\,, && -2.0 \leq [\mathrm{Fe/H}] \leq -0.3\,,\\
&J-H \propto 0.14 \pm 0.01[\mathrm{Fe/H}]\,, && -2.0 \leq [\mathrm{Fe/H}] \leq -0.3\,,\\
&H-K = 0.08\,, && -2.0 \leq [\mathrm{Fe/H}] \leq -0.8\,,\\
&H-K \propto 0.09 \pm 0.03[\mathrm{Fe/H}]\,, && -0.8 \leq [\mathrm{Fe/H}] \leq -0.3\,,\\
&J-H \propto 1.52 \pm 0.51(H-K)\,, && -0.6 \leq [\mathrm{Fe/H}] \leq -0.3\,.
\end{aligned}
\tag{3}
$$

These relationships were derived from large-aperture measurements of disk and bulge Galactic globular clusters by M. Malkan & M. Aaronson (1980, unpublished). The original data were dereddened using the values published in Armandroff (1989), which is also the source of our adopted [Fe/H] values. In Figure 6, a $\Delta(J-H)/\Delta(H-K)$ metallicity envelope based on the uncertainty in this relationship is shown. The large uncertainty in this relationship is caused by the small numbers of metal-rich Galactic globular clusters with large-aperture near-IR photometry and their relatively large scatter in $H-K$.

Based on the discussion in § 4.1.1, we assume our entire elliptical galaxy sample is at the high end of the Galactic globular cluster metallicity scale, and we adopt the nonconstant $H-K$/metallicity relationship appropriate for [Fe/H] > -0.8. This assumption is not critical to the conclusions of this paper, but it will be more important in Paper II.

4.1.3. *Intermediate-Age Populations*

As Persson et al. (1983) first demonstrated, the integrated near-IR colors of intermediate-age (1–3 Gyr) Magellanic Cloud star clusters are much redder than are the integrated colors of old clusters because of the presence of an extended AGB (see also Frogel, Mould, & Blanco 1990). These intermediate-age Magellanic Cloud clusters have subsolar ([Fe/H] ≈ -0.7) metallicities, however, while the mean metallicity of luminous elliptical galaxies is typically estimated to be solar or above (Peletier 1989; Gorgas, Efsta-

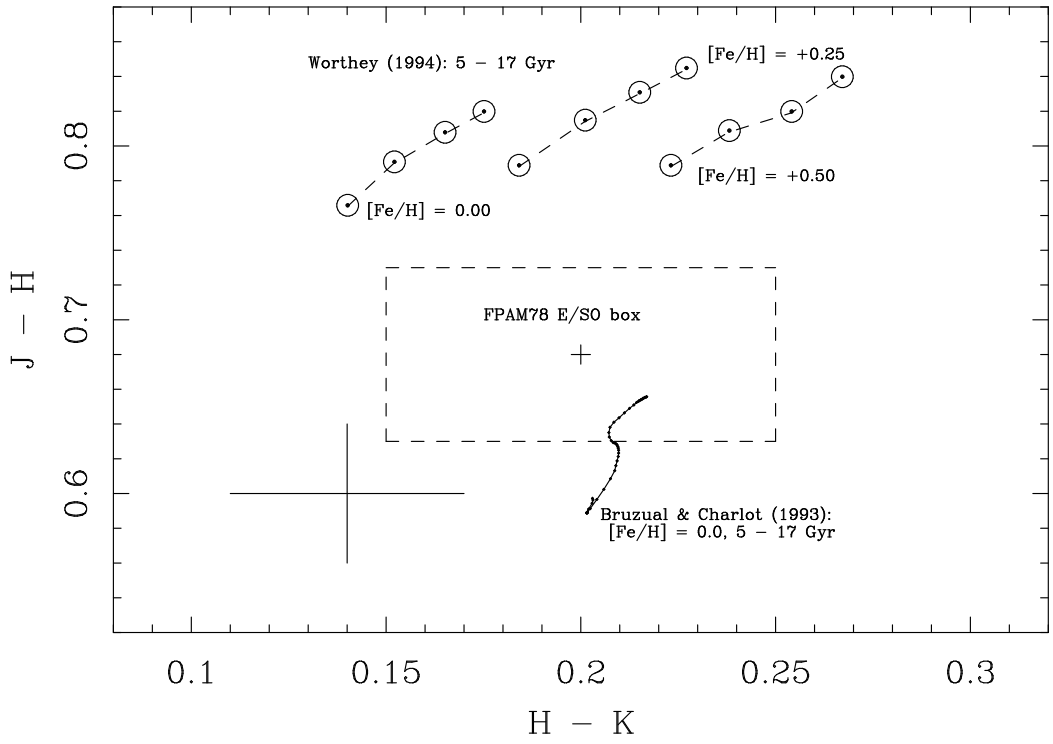

FIG. 5.—Bruzual & Charlot (1993) and Worthey (1994) models for ages 5–17 Gyr compared with FRAM78 E/S0 large-aperture colors. Both the model colors and the FPAM78 colors are reported to be on the CIT system by the cited authors. The typical FRAM78 error bar is shown in the bottom left corner. Models get redder as they get older. Not only do these models disagree with each other, but they also do not reproduce the near-IR colors of real galaxies.

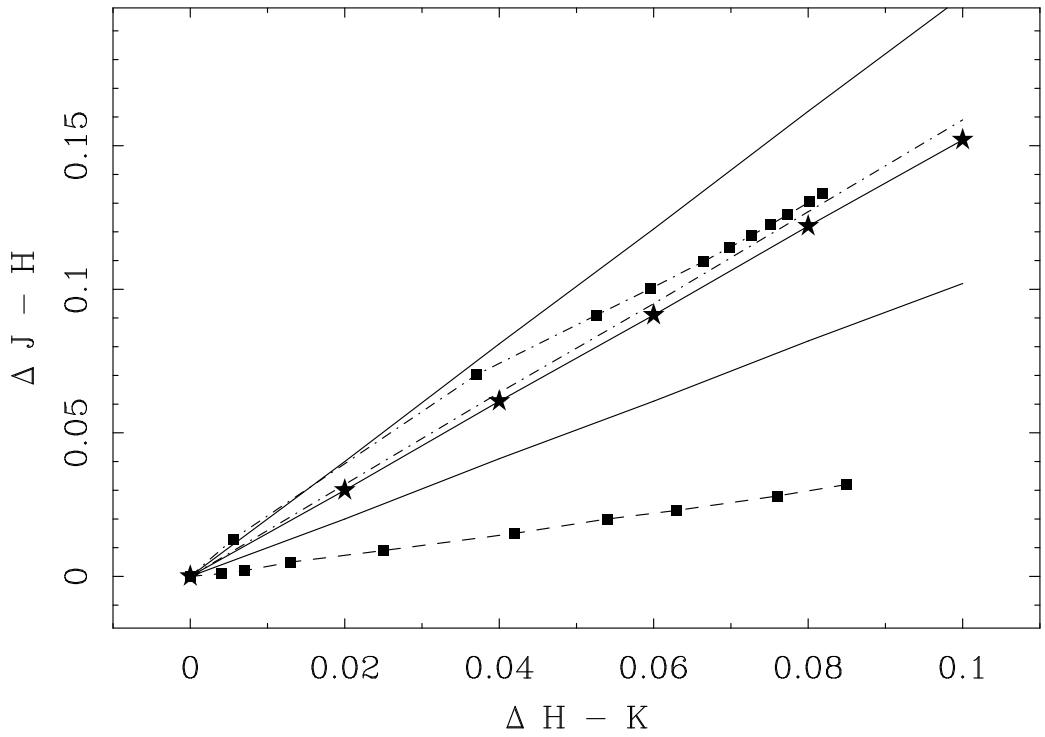

FIG. 6.—Vectors illustrating the effects of increasing metallicity, intermediate-age light, and internal reddening in the near-IR color-color plane. The origin of these vectors is given in the text. The middle solid line (with stars) is the mean Galactic globular cluster color-metallicity relationship, while the outer solid lines delineate the envelope created by the uncertainty in that relationship. The dot-dashed line with filled squares illustrates the internal reddening effects of the Wise & Silva (1996) star-dust mixture model described in the text. Each interval between the squares represents a change of $A_V \approx 5$. The dot-dashed line (without squares) illustrates the effects of a simple screen model (based on the reddening law of Cardelli, Clayton, & Mathis 1988). The dashed line with squares illustrates the effects of increasing intermediate-age AGB light as described in the text.

thiou, & Salamanca 1990; Worthey, Faber, & González 1992; Davies, Sadler, & Peletier 1992). As metallicity increases, how are the colors of intermediate-age clusters affected?

Unfortunately, there is no certain answer to this question. There are no solar-metallicity star cluster analogs in the Milky Way system to the subsolar-metallicity intermediate-age clusters in the Magellanic Clouds, so this question cannot be addressed directly. Most currently available models of intermediate-age/intermediate-mass stellar evolution are not very helpful because either they do not reproduce the known characteristics of the Magellanic Cloud intermediate-age clusters or they do not span a range of metallicity.

Vassiliadis & Wood (1993) have published the most successful and complete models (see the Habig 1996 critical review) in that they can reproduce the AGB tip bolometric luminosities of the Magellanic Clouds clusters with main-sequence turnoff (MSTO) masses less than 2.5 $M_{\odot}$. These models make two predictions about the solar-metallicity extended AGB. First, the bolometric luminosity of the solar-metallicity extended AGB tip will be about -5.3 or ~ 0.2 mag *fainter* than in the Magellanic Clouds, which is still well above the tip of the solar-metallicity FGB ($M_{\rm bol} \sim -3.8$; see, e.g., Frogel, Cohen, & Persson 1983). Second, effective temperatures of solar-metallicity extended AGB stars will be *cooler* and therefore have redder near-IR colors than will the Magellanic Cloud extended AGB stars.

However, these Vassiliadis & Wood (1993) models do not produce carbon stars, the distinctive signature of intermediate-age populations in the Magellanic Clouds and the Galactic dwarf spheroidal galaxies. As they point out, this is a common failing of intermediate-mass stellar evolution models (see also Habing 1996). Carbon stars are thought to be formed via dredge-up during the pulsation phases of the AGB period (Iben & Renzini 1983). The dredge-up process described by Iben & Renzini becomes less efficient as metallicity increases, reducing the C/M extended AGB star ratio. The enhancement of carbon in the stellar photospheres of extended AGB stars produces spectacular spectroscopic features, but it does not significantly affect their evolution or gross physical characteristics (cf. Habing 1996)—these stars should be cooler and bolometrically brighter than the FGB tip, regardless of whether or not they are C or M stars.

We adopt, then, the following hypothesis, based on the best available models: for the age range of 1–3 Gyr, as metallicity increases to values above the Magellanic Cloud mean, (1) the AGB tip bolometric luminosity decreases but still remains much brighter than the FGB tip; (2) the effective temperature of intermediate-age AGB stars decreases, and therefore the mean color of the extended AGB becomes redder; and (3) C/M star ratio will decrease.

In the absence of compelling evidence to the contrary, we expect that solar-metallicity intermediate-age star clusters will have redder near-IR colors than will their Magellanic Cloud counterparts. However, we are unable to estimate magnitude of this effect in a meaningful way. To be conservative, below we have elected to use intermediate-age Magellanic Cloud cluster colors to represent the colors of an intermediate-age stellar population within an elliptical galaxy.

4.1.4. *Intermediate-Age Vector*

We have simulated the color effect of adding an increasing amount of intermediate-age stars to an old stellar population in Table 3. The "old population" colors are merely the mean, large-aperture colors of elliptical galaxies taken from SS92 and FPAM78 for the optical and near-IR colors, respectively. The "intermediate population" colors are mean, large-aperture colors for SWB class IV–IV intermediate-age Magellanic Cloud clusters, computed from data in van den Bergh (1981) and Persson et al. (1983) for the optical and near-IR colors, respectively. Since we expect an intermediate-age population within an elliptical galaxy to have higher mean metallicity than the Magellanic Clouds and, thus, redder near-IR colors, the effect of using Magellanic Cloud cluster colors in this simulation will be to *overestimate* the amount of AGB light (and therefore mass) needed to produce a color change relative to a purely old stellar population. We discuss this issue further in § 5.1. The adopted colors are listed in Table 3.

Using these adopted values, we can simulate the effects of increasing the fractional amount of K-band light on the colors of an old population. Photometric properties are computed using the following set of equations:

$$\frac{F_Y^K}{F_O^K} = \text{input} ,$$

$$\frac{F_Y^J}{F_O^J} = \frac{(F_Y^J/F_Y^K)(F_Y^K/F_O^K)}{F_O^J/F_O^K} ,$$

$$\frac{F_Y^K}{F_T^K} = 1 - \left(1 + \frac{F_Y^K}{F_O^K}\right)^{-1} ,$$

$$(J-K)_T = -2.5 \log \left[\frac{F_O^J}{F_O^K} \frac{1 + (F_Y^J/F_O^J)}{1 + (F_Y^K/F_O^K)}\right] . \quad (4)$$

Quantities related to the old stellar population are denoted by the subscript O, to the younger population stellar population by the subscript Y, and to the mixture of the two by the subscript T. The superscripts denote the relevant photometric bands. Thus, equation (4) is written in terms of J and K bands. Similar equations can be written for any other photometric combination.

TABLE 3

ADOPTED INTEGRATED COLORS

Age (1)	$U-B$ (2)	$B-V$ (3)	$J-H$ (4)	$H-K$ (5)	$J-K$ (6)	M/L_K (7)
Old (10 Gyr)	0.60	0.90	0.67	0.22	0.89	1.30
Intermediate (2 Gyr).....	0.16	0.59	0.72	0.35	1.07	0.60

NOTES.—Cols. (1)–(6): see discussion in § 4.1.4; col. (7): see discussion in § 5.1.

TABLE 4

SIMPLE INTERMEDIATE-AGE/OLD MIXTURE MODEL

F_Y^K/F_T^K (1)	M_Y^K/M_T^K (2)	$\Delta(J-H)$ (mag) (3)	$\Delta(H-K)$ (mag) (4)	$\Delta(U-B)$ (mag) (5)	$\Delta(B-V)$ (mag) (6)	$\Delta(U-V)$ (mag) (7)
0.00.....	0.00	0.000	0.000	0.00	0.00	0.00
0.03.....	0.01	0.001	0.004	−0.02	−0.01	−0.03
0.06.....	0.03	0.002	0.007	−0.04	−0.02	−0.06
0.09.....	0.04	0.004	0.011	−0.06	−0.03	−0.10
0.13.....	0.06	0.006	0.016	−0.09	−0.05	−0.14
0.17.....	0.08	0.007	0.021	−0.11	−0.06	−0.17
0.20.....	0.10	0.009	0.025	−0.13	−0.07	−0.20
0.33.....	0.19	0.015	0.042	−0.20	−0.12	−0.32
0.43.....	0.26	0.020	0.054	−0.25	−0.15	−0.39
0.50.....	0.32	0.023	0.063	−0.28	−0.17	−0.45
0.60.....	0.41	0.028	0.076	−0.32	−0.20	−0.52
0.67.....	0.48	0.032	0.085	−0.34	−0.22	−0.56
1.00.....	1.00	0.050	0.130	−0.44	−0.31	−0.75

NOTES.—Col. (1): Ratio of younger stellar population flux to total flux, K band (see eq. [4]). Col. (2): Ratio of younger stellar mass to total mass (see eq. [5]). Cols. (3)–(7): Change in indicated colors relative to colors of purely old stellar population.

The numerical results of this simulation are listed in Table 4. The resultant near-IR two-color vector is drawn in Figure 6. This simple simulation has higher near-IR fidelity than optical fidelity, given the relatively greater sensitivity of optical colors to the exact details of age, metallicity, and horizontal-branch morphology. It also places no constraints on the origins of such an intermediate-age population, only on its current fractional photometric contribution.

An issue for the present study is whether a red integrated $H-K$ color is a sign of an intermediate-age AGB or of enhanced light elements. Qualitatively, the Ti-enhanced BW M stars are as red as $H-K = 0.45$, or roughly 0.05–0.1 mag redder in $H-K$ than are field M giants at similar $J-H$ color, and reach $M_K \approx -8$ (Frogel & Whitford 1987; Tiede et al. 1995). In contrast, extended AGB stars in Magellanic Cloud clusters ([Fe/H] ~ -0.7) have $H-K$ colors in the range 0.3–0.8 and M_K in the range -8.5 to -9.0, i.e., much redder than the reddest BW M stars at similar absolute magnitudes (Frogel et al. 1990). As discussed above, we expect higher metallicity extended AGB stars to be even redder. Clearly, a small population of intermediate-age stars will have a significantly larger near-IR color effect than will a small population of Ti-enhanced stars. This issue becomes most important when interpreting central colors, as discussed in Paper II.

4.2. *Internal Reddening*

The effects of dust on the colors elliptical galaxies have been extensively discussed recently by Witt et al. (1992), Goudfrooij & de Jong (1995), Wise & Silva (1996, 1998), and Silva & Wise (1996). These papers highlight the importance of differentiating between foreground screen models and models that mix stars and dust homogeneously.[5]

4.2.1. *Internal Reddening Vector*

To illustrate how dust can redden near-IR colors, we show two reddening vectors in Figure 6. First, we show the effects of a screen model. The slope of this line was derived from Cardelli, Clayton, & Mathis (1989; see their Table 3). The second line was adopted from the dust-star mixture models presented in Wise & Silva (1996). For this latter vector, we chose $(\alpha, \gamma) = (1.0, 1.5)$ (see Fig. 8 in Wise & Silva 1996). The most noticeable difference between this model and a screen model is that the mixture model requires much more dust to achieve the same reddening effect than does the screen model. The resultant dust reddening vector is drawn in Figure 6. Note that these reddening vectors lie within the metallicity envelope but are separated from the increasing AGB light vector.

NGC 3607 appears to be the galaxy most affected by significant internal reddening in our sample. This $S0_3(3)$ galaxy was included in our sample because it is a close companion to one of our original sample elliptical galaxies, NGC 3605. Fortuitously, it has the reddest $J-K$ and $H-K$ colors of any galaxy in our sample (see Figs. 3 and 4), although its $J-H$ color is not atypical. This galaxy is known to contain an extensive dust ring, as well as spatially extended central Balmer emission, which may be organized as a rapidly rotating ring or disk (Singh et al. 1994; Fisher, Franx, & Illingworth 1996). Singh et al. concluded that the Balmer emission was driven by young stars. Although it seems most likely that the near-IR colors of this galaxy are caused by significant internal reddening, we note that this galaxy is not displaced along a simple dust screen model reddening vector (see Fig. 6). Perhaps that is not surprising: the spatial distribution of the observed dust feature and the known effects of more complex star-dust mixtures (cf. Witt et al. 1993; Wise & Silva 1996) will naturally produce a more complicated reddening trajectory than will a simple foreground dust screen model.

5. CONSTRAINTS ON AMOUNT OF INTERMEDIATE-AGE STELLAR MASS

5.1. *Methodology and Results*

The elliptical galaxies observed here classified as "young" by virtue of their global morphology and/or

[5] As discussed in Wise & Silva (1998), the K-band contribution from the thermal emission of warm dust in these elliptical galaxies is expected to be negligible, even in their central regions where the stellar radiation field is most intense and the dust density is presumably at its maximum value. Thus, we disregard the possible contribution of thermal dust emission in the K band in this paper.

TABLE 5

PREDICTED NEAR-IR COLORS DIFFERENCES

NGC (1)	Σ (2)	$\Delta(U-B)_{e,0}$ (obs) (3)	$\Delta(B-V)_{e,0}$ (obs) (4)	$\Delta(U-V)_{e,0}$ (obs) (5)	$\Delta(J-H)_{e,0}$ (predicted) (6)	$\Delta(H-K)_{e,0}$ (predicted) (7)	$M_I/M_{\rm Total}$ (predicted) (8)	SS92 Type (9)
Most morphologically disturbed:								
596.....	4.60	−0.072	−0.036	−0.107	0.005	0.013	0.05	G_T, Hβ
3610.....	7.60	−0.060	−0.078	−0.130	0.006	0.016	0.06	G_1, Hβ
3640.....	6.85	−0.024	−0.023	−0.046	0.001	0.005	0.02	G_1, Hβ
4125.....	6.00	−0.018	−0.019	−0.035	0.001	0.004	0.01	G_1, Hβ
4915.....	6.48	−0.037	−0.034	−0.071	0.002	0.008	0.03	G_1, Hβ
Less morphologically disturbed:								
636.....	1.48	−0.005	−0.020	−0.025	0.001	0.004	0.01	G_3, Hβ
1700.....	3.70	−0.026	−0.031	−0.055	0.002	0.007	0.03	G_2, Hβ
3156.....	1.70	−0.147	−0.177	−0.325	0.015	0.042	0.19	G_0, Hβ
3377.....	1.48	−0.076	−0.047	−0.124	0.005	0.013	0.05	G_0, Hβ
4697.....	0.00	−0.090	−0.022	−0.111	0.004	0.012	0.04	G_0
5322.....	2.00	−0.053	−0.047	−0.098	0.004	0.011	0.04	G_2, Hβ
Ongoing merger:								
3921.....	8.8	−0.2	−0.2	−0.4	...	...	...	Merger

NOTES.—Col. (1): NGC number. Col. (2): Morphological fine-structure parameter from SS92. Larger numbers equal more structure. Col. (3): Observed $U-B$ color difference between galaxy and mean color for galaxies of similar M_B from SS92. Col. (4): Observed $B-V$ color difference between galaxy and mean color for galaxies of similar M_B from SS92. Col. (5): Observed $U-V$ color difference between galaxy and mean color for galaxies of similar M_B from SS92. Col. (6): Predicted $J-H$ color difference, if optical color differences are caused by presence of intermediate-age stellar population only. Predictions based on model presented in Table 4. Col. (7): Predicted $H-K$ color difference, if optical color differences are caused by presence of intermediate-age stellar population only. Predictions based on model presented in Table 4. Col. (8): Predicted ratio of intermediate-age stellar mass to total stellar mass, if optical color differences are caused by presence of intermediate-age stellar population only. Predictions based on model presented in Table 4. Col. (9): SS92 merger type classification. See Table 1. NGC 3921 data from Schweizer 1996. No near-IR color difference predicted for NGC 3921 since it is too young. See text.

optical colors by SS92 are listed in Table 5. If it is assumed that all the additional blue light originates from an intermediate-age population, the optical colors listed in Table 4 and the model presented in Table 3 can be used to estimate a corresponding near-IR color enhancement and the total amount of intermediate-age stellar mass. This assumption is similar to the SS92 assumption that all the blue light originates in a younger population, although here we restrict the implied age range more tightly.

To estimate the fractional mass contribution of the intermediate-age stellar population, we first solve equation (4) and then the following equations:

$$\frac{M_Y^K}{M_O^K} = \frac{F_Y^K}{F_O^K}\frac{(M/L)_Y^K}{(M/L)_O^K}, \quad \frac{M_Y^K}{M_T^K} = 1 - \left(1 + \frac{M_Y^K}{M_O^K}\right)^{-1}. \qquad (5)$$

We assume that the old and intermediate-age populations have mean M/L_K of 1.30 and 0.60, respectively (Worthey 1994; but see discussion below).

The estimates are listed in Table 5. Comparison of the estimated near-IR color changes and the observed near-IR colors (Figs. 3 and 4) shows that if an intermediate-age population is present, it can only account for roughly 10% of the total stellar mass. In fact, given the observational error bars, the observed near-IR colors are consistent with *none* of the stellar mass being intermediate-age (1–3 Gyr). *In short, the aggregate global optical and near-IR color data are consistent with 90%–100% of the luminous stellar mass being old and metal-rich.* However, these photometric data do not offer much insight into whether the mean stellar age is 5 or 15 Gyr. It is only certain that the events that caused the morphological fine structure observed in these galaxies did not produce a significant globally distributed intermediate-age stellar population.

These estimated upper limits on intermediate-age mass fraction can be affected by two systematic problems. First, we do not know the true near-IR color of a metal-rich intermediate-age stellar population. However, since we expect such a population to have redder colors than the Magellanic Cloud clusters colors we have used, we also expect that we have overestimated the amount of light and, therefore, the mass needed to make an observable change in integrated color. Thus, the true mass fraction upper limits are likely to be smaller than the constraints given above.

Our mass fraction estimate is more affected by uncertainties in the adopted K-band M/L's. Unfortunately, these values were adopted from models (Worthey 1994) that we have already noted do not correctly reproduce near-IR elliptical colors. Thus, it seems likely that K-band M/L values estimated from these models are uncertain. To illustrate the potential magnitude of this problem, consider the Worthey (1994) model grid. For the metallicity range $-0.25 \le [\mathrm{Fe/H}] \le 0.25$ and an age range of 1.5–5 Gyr (i.e., our "intermediate-age" population), the K-band M/L range is 0.45–0.80. For the same metallicity range and an age range of 12–17 Gyr (i.e., our "old" population), the K-band M/L range is 0.90–1.65. We adopted the middle of these ranges, i.e., 0.60 and 1.30, respectively. The most extreme changes in estimated mass fraction would occur if we choose the intermediate-age and old K-band M/L value pairs to be (0.45, 1.65) and (0.80, 0.90). If we substitute these extreme values into the simulation presented in Table 4, at a value of $F_Y^K/F_T^K = 0.33$, M_Y^K/M_T^K becomes 0.12 and 0.31, respectively, compared with the value of 0.21 listed in Table 3. For the other values of F_Y^K/F_T^K, M_Y^K/M_T^K changes by roughly the same relative amount. While these are clearly the most extreme excursions, they do illustrate that each of our mass fraction estimates are really in the middle of some unknown mass fraction range.

5.2. *Discussion*

Perhaps the low global intermediate mass fraction estimates are not surprising given the results of merger models

that account for gasdynamic effects (e.g., Mihos & Hernquist 1996; Barnes & Hernquist 1996). A ubiquitous feature of these models is the dissipative flow of gas to the center of the newly formed potential well, where densities become high enough that a burst of star formation is possible. In other words, mergers that include gas produce star formation events that are centrally concentrated, not globally distributed. Some star formation does occur in the tidal tails thrown off by the merger events, and this younger material might fall back into the merger product for a long time. While this would produce a more globally distributed younger stellar component, it accounts for very little of the total mass of the final galaxy (Hibbard & Mihos 1995). Nevertheless, the amount of newly formed stellar mass only amounts to $\sim 5\%$ of the total progenitor masses (J. C. Mihos 1996, private communication). Furthermore, these newly formed stars will be concentrated in the central regions of the galaxies. We focus on these important points in Paper II, where we study the central regions of our sample galaxies in more detail and discover two obvious cases of centrally concentrated AGB light.

5.2.1. *An Example: NGC 3921*

The ongoing merger NGC 3921 (variously known as Arp 224, Mrk 430, VV 31, I Zw 28) is the most morphologically extreme galaxy in our sample. It has an A-type spectrum and blue continuum (Schweizer 1978, 1996; Kennicutt 1992) and is often compared with the poststarburst "E + A" galaxies seen at higher redshift (Dressler & Gunn 1983). Its properties have been extensively characterized by Schweizer (1996). These properties leave little doubt that NGC 3921 was formed by a major disk-disk merger event and that star formation peaked roughly 1 Gyr ago, at least in the nucleus.

Yet, within the observation uncertainties, NGC 3921 has the same global near-IR colors, $(J-H)_0 = 0.63$ and $(H-K)_0 = 0.21$ (see Table 2), as the other galaxies in our sample (see Fig. 2), suggesting that the integrated near-IR light of this proto–elliptical galaxy is dominated by old, metal-rich stars that originated in the merger progenitors. Why does this galaxy not have redder $H-K$ colors? The presence of strong Balmer lines suggests that the merger-driven star formation event is about 1 Gyr old (Schweizer 1996), too old for a significant young, red supergiant component, but too young for a significant intermediate-age AGB component. This illustrates the narrowness of the age range to which $H-K$ is sensitive. It also underscores that most of the stellar mass in such spectacular merger events is old and being donated by the progenitor galaxies, as pointed out by SS92 and seen in models of major mergers discussed above.

5.2.2. *Counterexample: M32 (=NGC 221)*

The existence of an intermediate-age stellar population in M32 was first suggested by O'Connell (1980). This conclusion was supported by the studies of Burstein et al. (1984), Rose (1985), and Bica, Alloin, & Schmidt (1990). The discovery of an extended giant branch population by Freedman (1992) and Elston & Silva (1992) seemed to confirm the existence of an intermediate-age population in M32. The observed extended giant branch was argued to be the AGB counterpart to the intermediate-age MSTO first suggested by O'Connell.

How does the presence of these extended giant branch stars affect the global colors of M32? As Figures 3 and 4 demonstrate, M32 has an extreme $H-K$ (and therefore an extreme $J-K$) color relative to its total mass (i.e., central velocity dispersion) and metric luminosity (i.e., $\log D_N$). This is the expected signature of a significant intermediate-age stellar population.

Using the simple, schematic model presented in Table 4, we can estimate the fractional stellar mass contribution of this intermediate-age population. From Figures 3 and 4, $\Delta(J-K)$ and $\Delta(H-K)$ are 0.08 and 0.06 mag, respectively. Each color difference has an uncertainty of ~ 0.02 mag. Table 4 suggests that these color differences correspond to a fractional intermediate-age stellar mass contribution of 20%–40% within a circular area with diameter D_N.

Is this estimate consistent with past estimates? Rose (1985) concluded that at 4000 Å, 50% of the central light of M32 came from an intermediate-age (~ 5 Gyr), roughly solar-metallicity population, and the rest from an old (>10 Gyr), solar-metallicity population. Using the B-band M/L values listed in Table 5 of Worthey (1994), the fractional luminosity contribution of the intermediate-age component can be converted into a fractional stellar mass contribution of $\sim 30\%$. Likewise, Bica et al. (1990) estimated that the intermediate-age component contributed $\sim 30\%$ of the light at 5870 Å. Using the V-band M/L values from Table 5 in Worthey (1994), this fractional luminosity contribution can be transformed into a fractional stellar mass contribution of 19%. Given the various uncertainties involved in these estimates, we conclude that the derived fractional stellar mass contribution derived from the near-IR colors and the simple model in Table 4 are in agreement with the Rose and Bica et al. results.

Following the rationale of SS92, the model discussed in Table 3, and various past population synthesis studies, one might expect that M32 has very blue colors for its luminosity and/or stellar mass. We examine this question in two ways. First, we can make the same comparison between observed color and mean color that SS92 made for all the galaxies in their sample. Using the SS92 methodology, we compute $\Delta(U-B)_{e,0}$ and $\Delta(B-V)_{e,0}$ for M32. Adopting a distance modulus of 24.2 for M32, we convert B_T^0 to $M_B = -15.48$. Using the mean optical color-magnitude relations listed in Table 2 of SS92, we compute nominal $U-B$ and $B-V$ colors of 0.32 and 0.87, respectively, for this M_B. Given computed values of $(U-B)_{e,0}$ and $(B-V)_{e,0}$ of 0.42 and 0.89, the resultant $\Delta(U-B)_{e,0}$ and $\Delta(B-V)_{e,0}$ values are $+0.10$ and $+0.02$. In short, M32 has *redder UBV* colors than the extrapolated SS92 color-magnitude relationships would predict for its M_B, not bluer, as is expected if the intermediate-age population is dominating the optical colors in the way expected by SS92. Perhaps the SS92 color-magnitude relationships cannot be extrapolated to M32's absolute blue magnitude or the derived M32 absolute blue magnitude is wrong. The latter possibility seems unlikely since the M_B would have to be several magnitudes brighter to make $\Delta(U-B)_{e,0}$ and $\Delta(B-V)_{e,0}$ as large as our empirical model and the estimated $\Delta(J-H)$ and $\Delta(H-K)$ colors suggest.

A second approach is to compare the optical colors of M32 to the more global $(B-V)_0$–$\log \sigma$ relationship, as discussed in Burstein et al. (1987) and Bender, Burstein, & Faber (1993). As the latter paper illustrates (see, e.g., their Fig. 6), M32 is indeed bluer in $B-V$ than the mean color for its $\log \sigma$, consistent with the presence of an intermediate-age population. However, it is also apparent that the scatter

in $B-V$ for such low stellar mass elliptical galaxies is quite large, weakening the concept of a "mean" color.

6. ON THE ORIGIN OF BLUE LIGHT IN DISTURBED ELLIPTICAL GALAXIES: METALLICITY SCENARIOS

The lack of a significant, distributed AGB population within $R < 1.5R_e$ is inconsistent with the SS92 suggestion that the excess blue light observing in this region comes primarily from a population of A–F stars created in a major merger event 1–5 Gyr ago. If this were the case, we should have detected the residue of this event via its associated AGB population. While it is possible that the excess blue light is coming from a stellar population that is less than 1 Gyr old, we view this to be unlikely, as no other indicators of such a young population have been observed.

Metallicity effects are the obvious alternative origin of the observed excess blue light. SS92 considered the possibility of such effects to be less likely than the presence of a younger population, so they did not explore metallicity effects in their models. Here we consider two possible metallicity-driven origins for the excess blue light observed by SS92: the accretion of a metal-poor population and the photometric effects of relative abundance difference.

6.1. *Accreted Stars*

Models of dissipationless accretion events illustrate that unequal-mass mergers are quite capable of producing structure similar to the observed morphological fine structure. Moreover, the stellar mass from the disrupted satellite is globally distributed. Since less luminous, less massive companions are also likely to be bluer because of the color-magnitude effect, this disruption and global redistribution provides a natural mechanism for lowering the mean metallicity and making the net galaxy bluer. The observation that shells in these galaxies tend to either equivalent color or bluer than the surrounding stellar material lends support to this scenario (Fort et al. 1986; Schombert & Wallin 1987; McGaugh & Bothun 1990; Forbes, Reitzel, & Williger 1995).

Table 6 presents a simple model for adding metal-poor stellar mass to some precursor galaxy with redder colors. The precursor absolute magnitude was chosen to be $M_B = -21.4$, i.e., similar to NGC 3610, the most disturbed galaxy in our sample. The precursor color was calculated from the SS92 color-magnitude relationships. The simple accretion model presented in Table 6 is calculated from the following set of equations:

$$\begin{aligned} F_V^F &= F_V^P + F_V^S \equiv 1 , \\ F_B^F &= F_B^P + F_B^S , \\ F_B^P &= F_V^P \, 10^{-0.4(B-V)^P} , \\ F_B^S &= 10^{-0.4(B-V)^F} - F_B^P , \end{aligned} \tag{6}$$

where $(B-V)^P$, F_V^P, and F_B^P are the $B-V$ color of the precessor galaxy and the fractional V- and B-band contributions it makes to the final galaxy. Equivalent quantities are defined for the satellite galaxy being accreted (superscript S) and the final resultant galaxy (superscript F). These equations can be used to calculate the satellite color necessary to make the final color bluer than the parent color by a specified amount once $(B-V)^P$ and $(B-V)^F$ are specified. To compute Table 6, $(B-V)^P$ and $(B-V)^F$ were set to 0.94 and 0.86. $(B-V)^P$ is the mean elliptical color for $M_B = -21.37$ (the absolute blue magnitude of NGC 3610), calculated from the SS92 color-magnitude relationships, while $(B-V)^F$ is the actual color of NGC 3610. By varying, F_V^P, all other quantities in Table 6 can be calculated using equation (6). This simple model illustrates that a range of relative photometric contributions and, therefore, a range of relative

TABLE 6

EXAMPLE ACCRETION MODEL

PRECURSOR (F_V) (1)	SATELLITE (F_V) (2)	PRECURSOR (F_B) (3)	SATELLITE (F_B) (4)	SATELLITE $B-V$ (5)	SATELLITE [Fe/H] (6)
0.950	0.050	0.400	0.052	−0.043	...
0.900	0.100	0.379	0.073	0.341	...
0.850	0.150	0.358	0.094	0.506	...
0.800	0.200	0.337	0.115	0.599	−2.000
0.750	0.250	0.316	0.136	0.659	−1.750
0.700	0.300	0.295	0.157	0.701	−1.500
0.650	0.350	0.274	0.178	0.732	−1.250
0.600	0.400	0.253	0.199	0.756	−0.750
0.550	0.450	0.232	0.220	0.775	...
0.500	0.500	0.211	0.242	0.790	...
0.450	0.550	0.190	0.263	0.803	−0.600
0.400	0.600	0.168	0.284	0.814	...
0.300	0.700	0.126	0.326	0.831	...
0.200	0.800	0.084	0.368	0.844	...
0.100	0.900	0.042	0.410	0.854	−0.300
0.005	0.995	0.002	0.450	0.862	...

NOTES.—Col. (1): Fraction of final V-band light from precursor. Col. (2): Fraction of final V-band light from accreted satellite. Col. (3): Fraction of final B-band light from precursor. Col. (4): Fraction of final B-band light from accreted satellite. Col. (5): Required satellite $B-V$ color to create specified final color. Col. (6): Adopted metallicity of accreted satellite. Assumes Galactic globular cluster color-metallicity relationship (see text). Precursor galaxy assumed to have $M_B = -21.4$ and $B-V = 0.94$. Precursor galaxy color derived from color-magnitude relationship derived by SS92. Color of final galaxy (precursor + satellite) assumed to be $B-V = 0.86$. See text for further information.

masses, can produce the observed colors without invoking significant star formation.

6.2. *Relative Abundance Differences*

A second possibility is a relative abundance difference. Consider NGC 5322, for example. Unlike many other field elliptical galaxies, NGC 5322 appears to have [Mg/Fe] ≈ 0 at all radii. As this is consistent with the mean [Mg/Fe] observed in current-epoch spiral galaxies, Bender (1996) has argued that NGC 5322 is one of the best disk-disk merger remnant candidates. How would a relative difference in [Mg/Fe] translate into a relative color difference? Assume that [Mg/Fe] is a tracer of [α/Fe], and consider the following two scenarios:

1. *Total metallicity conserved.*—Here, as [Mg/Fe] increases, [Fe/H] will decrease. Since main-sequence stars and lower giant branch stars contribute about equal amounts of light at 5000 Å, metallicity effects on both subpopulations must be considered. Increased [α/Fe] will make MSTO stars cooler (and therefore redder) because of changes in mean central opacity (VandenBerg 1988). Decreased [Fe/H] will make them bluer as a result of decreased line atmospheric line blanketing. Furthermore, since the ratio of electron donation to H^- is 2:1 for Mg and Fe in the envelopes of FGB stars (Renzini 1977), an increasing [Mg/Fe] but decreasing [Fe/H] will have a warming effect on the giant branch due to decreased envelope opacity, making it bluer.

2. *Total metallicity is not conserved.*—In this scenario, as [Mg/Fe] increases, [Fe/H] remains constant or increases. Increasing [α/Fe] coupled with constant or increasing [Fe/H] will make the MSTO redder. Since Mg + Fe is absolutely increasing, the giant branch will also become redder.

For the first case, it is very difficult to estimate either the magnitude or the sense of broadband color effects without detailed stellar atmosphere and interior models. The photometric effects of the second case, however, can be estimated in a straightforward manner. Assume that $\Delta[Z/Z_\odot] \propto \Delta[\mathrm{Mg/Fe}] = 0.3$. Using the readily accessible Worthey (1994) single-burst stellar population models, at $T = 12$ Gyr, this metallicity change corresponds to $\Delta(U-B) \approx 0.12$ and $\Delta(B-V) \approx 0.07$ for [Fe/H] ≤ 0.0. In comparison, NGC 5322 has optical color offsets of $\Delta(U-B) = 0.053$ and $\Delta(B-V) = 0.047$ from the mean color-magnitude relationship derived by SS92.

Given the uncertainties associated with such an estimate, we conclude that a relative abundance ratio difference could explain the NGC 5322 color offset reported by SS92. Obviously, more detailed modeling is required to confirm this conclusion. As Bender (1996) discusses, such normal [Mg/Fe] values lend support to the hypothesis that some disturbed elliptical galaxies are evolved disk-disk merger remnants since these [Mg/Fe] values are consistent with the abundance ratios observed in current-epoch spiral galaxies. However, given the amount of gas in current-epoch spiral galaxies, disk-disk mergers should also result in centrally concentrated younger stellar populations. As discussed in Paper II, the central region of NGC 5322 appears to contain such a young population, further strengthening the hypothesis that this galaxy at least was formed by a disk-disk merger.

7. SUMMARY

1. Regardless of the details of morphology and optical color, most of the galaxies observed in our sample have similar global near-IR color. The simplest interpretation of this result is that these galaxies have similar mean first-ascent giant branch properties with little or no evidence for an enhancement of cool AGB stars from an intermediate-age stellar population distributed within the region $R < 1.5R_e$.

2. A small amount of intermediate-age mass cannot be ruled out. We have used a simple model and self-consistency checks to argue that regardless of their morphological fine structure, no more than $\sim 10\%$ of the mass in our sample elliptical galaxies can be of intermediate age. Conversely, the majority ($\gtrsim 90\%$) of the stellar mass in these objects must be old ($T > 10$ Gyr) and metal-rich ([Fe/H] > -0.3). The largest uncertainty in these estimates comes from the uncertainty in our adopted K-band M/L values.

3. However, given our observation errors, the data are in fact consistent with *all* the stellar mass being old and metal-rich. We argue that the enhanced blue light observed in many of these galaxies could be caused by metallicity effects, not by the presence of a younger stellar population as suggested by SS92. We propose two mechanisms: the accretion of a lower luminosity lower metallicity companion or a relative abundance difference between these blue galaxies and galaxies of similar M_B.

4. The global optical and near-IR photometric data imply that most of the stellar mass must have formed at high redshift. However, these data in no way constrain the "assembly era" of these galaxies. These galaxies could have been assembled in a hierarchical manner at any time in the last 10 Gyr, perhaps via the process outlined in Pascarelle et al. (1996).

As Bender (1996) highlighted, the apparent relative abundance differences between elliptical galaxies could arise naturally if some elliptical galaxies were assembled from galaxies akin to current-epoch spiral galaxies and some did not. Since spiral galaxies in general have significant gas masses, even at the present epoch, one would expect that disk-disk mergers would also lead to a central star formation event. In this scenario, the central regions of the merger product should have a younger mean stellar age than should its outer regions. Thus, the central 500 pc of these field elliptical galaxies, not a more extended region, may provide the best insight into the nature of the last merger event: whether it involved a significant quantity of gas or whether it was dissipationless accretion event.

Much of the debate around the nature of the mergers that are responsible for the observed morphological fine structure revolves around their magnitude and severity. In this paper, we have tested the hypothesis that gas-rich disk-disk mergers are responsible for the morphological fine structure characterized by SS92 by directly searching for the intermediate-age population that would be the current residue of a merger-induced star formation event. In general, our results do not support this hypothesis, as we have failed to find evidence for a correlation between morphological fine structure and the mean age of the stellar population. We thus favor the hypothesis that either (1) the major merger occurred more than 5 Gyr ago or (2) morphological fine structure and excess blue light is produced

through minor companion accretion events. Further support for this conclusion is presented in Paper II.

We thank Mike Merrill of the KPNO IR group for his assistance in using SQIID; Steve Shawl, Jim Hesser, and Cameron Reed, for sending us a digital version of their rationalized globular cluster photometry; and Stephane Charlot, Arjen Dey, Chris Mihos, Hans-Walter Rix, and Mike Wise for numerous helpful discussions. We also thank our referee, Jay Frogel, for helping us produce a better article. The observations and most of work to produce this article were done while D. R. S. was a KPNO staff astronomer. This research has made use of the NASA/IPAC Extragalactic Database (NED), which is operated by the Jet Propulsion Laboratory, California Institute of Technology, under contract with the National Aeronautics and Space Administration.

REFERENCES

Aaronson, M., Cohen, J. G., Mould, J., & Malkan, M. 1978, ApJ, 223, 824
Armandroff, T. 1989, AJ, 97, 375
Barnes, J. E. 1992, ApJ, 393, 984
Barnes, J. E., & Hernquist, L. 1996, ApJ, 471, 115
Bender, R. 1996, in New Light on Galaxy Evolution, ed. R. Bender & R. L. Davies (Dordrecht: Kluwer), 181
Bender, R., Burstein, D., & Faber, S. M. 1993, ApJ, 411, 135
Bender, R., Surma, P., Döbereiner, S., Möllenhoff, C., & Madejsky, R. 1989, A&A, 217, 35
Bica, E., Alloin, D., & Schmidt, A. A. 1990, A&A, 228, 97
Bothun, G. D., & Gregg, M. D. 1990, ApJ, 350, 73
Bothun, G., Romanishin, W., Strom, S. E., & Strom, K. M. 1984, AJ, 89, 1300
Bower, R. G., Lucey, J. R., & Ellis, R. S. 1992, MNRAS, 254, 601
Bressan, A., Chiosi, C., & Tantalo, R. 1996, A&A, 311, 425
Bruzual A., G., & Charlot, S. 1993, ApJ, 405, 538
Burstein, D. 1985, PASP, 97, 89
Burstein, D., Davies, R. L., Dressler, A., Faber, S. M., Stone, R. P. S., Lynden-Bell, D., Terlevich, R. J., & Wegner, G. 1987, ApJS, 61, 601
Burstein, D., Faber, S. M., Gaskell, C. M., & Krumm, N. 1984, ApJ, 287, 586
Burstein, D., & Heiles, C. 1984, ApJS, 54, 33
Cardelli, J. A., Clayton, G. C., & Mathis, J. C. 1989, ApJ, 345, 245
Charlot, S., Worthey, G., & Bressan, A. 1996, ApJ, 457, 625
Davidge, T. J. 1991, AJ, 101, 884
Davies, R. L., Burstein, D., Dressler, A., Faber, S. M., Lynden-Bell, D., Terlevich, R. J., & Wegner, G. 1987, ApJS, 64, 581
Davies, R. L., Sadler, E. M., & Peletier, R. F. 1993, MNRAS, 262, 650
de Vaucouleurs, G., de Vaucouleurs, A, Corwin, H. G., Buta, R. J., Paturel, G., & Fouqué, P. 1991, Third Reference Catalogue of Bright Galaxies (New York: Springer) (RC3)
Djorgovski, G., & Davis, M. 1987, ApJ, 313, 59
Dressler, A., & Gunn, J. E. 1983, ApJ, 270, 7
Dressler, A., Lynden-Bell, D., Burstein, D., Davies, R. L., Faber, S. M., Terlevich, R., & Wegner, G. 1987, ApJ, 313, 42
Elias, J. H., Frogel, J. A., Mathews, K., & Neugebauer, G. 1983, AJ, 87, 1029
Ellis, T., et al. 1993, Proc. SPIE, 1765, 94
Elston, R., & Silva, D. R. 1992, AJ, 104, 1360
Faber, S. M., Tremaine, S., Ajhar, E., Byun, Y.-I., Dressler, A., Gebhardt, K., Grillmar, C., & Kormendy, J. 1997, AJ, 114, 1771
Fisher, D., Franx, M., & Illingworth, G. 1996, ApJ, 459, 110
Forbes, D. A., Reitzel, D. B., & Williger, G. M. 1995, AJ, 109, 1576
Fort, B. P., Prieur, J.-L., Carter, D., Meatheringham, S. J., & Vigroux, L. 1986, ApJ, 306, 110
Freedman, W. L. 1992, AJ, 104, 1349
Frogel, J. A., Cohen, J. G., & Persson, S. E. 1983, ApJ, 275, 773
Frogel, J. A., Kuchinski, L. E., & Tiede, G. P. 1995, AJ, 109, 1154
Frogel, J. A., Mould, J., & Blanco, V. M. 1990, ApJ, 352, 90
Frogel, J. A., Persson, S. E., Aaronson, M., & Mathews, K. 1978, ApJ, 220, 75 (FRAM78)
Frogel, J. A., Persson, S. E., & Cohen, J. G. 1983, ApJS, 53, 713
Frogel, J. A., & Whitford, A. E. 1987, ApJ, 320, 199
González, J. J. 1993, Ph.D. thesis, Univ. California, Santa Cruz
Gorgas, J., Efstathiou, G., & Salamanca. A. A. 1990, MNRAS, 245, 217
Goudfrooij, P., & de Jong, T. 1995, A&A, 298, 784
Green, E. M., Demarque, P., & King, C. R. 1987, The Revised Yale Isochrones and Luminosity Functions (New Haven: Yale Univ. Obs.)
Gregg, M. D. 1989, ApJ, 337, 45
———. 1992, ApJ, 384, 43
Habing, H. J. 1996, A&A Rev., 7, 97
Hernquist, L., & Quinn, P. J. 1988, ApJ, 331, 682
———. 1989, ApJ, 342, 1
Hibbard, J. E., & Mihos, J. C. 1995, AJ, 110, 140
Iben, I., Jr., & Renzini, A. 1983, ARA&A, 21, 271
Illingworth, G. D., & Franx, M. 1989, in Dynamics of Dense Stellar Systems, ed. D. Merritt (Cambridge: Cambridge Univ. Press), 13
Kennicutt, R. C., Jr. 1992, ApJ, 464, 641
Kuchinski, L. E., & Frogel, J. A. 1995, AJ, 110, 2844
McGaugh, S. S., & Bothun, G. D. 1990, AJ, 100, 1073
McWilliam, A., & Rich, R. M. 1994, ApJS, 91, 749
Mihos, J. C., & Hernquist, L. 1996, ApJ, 464, 641
O'Connell, R. W. 1980, ApJ, 236, 430
Pascarelle, S. M., Windhorst, R. A., Keel, W. C., & Odewahn, S. C. 1996, Nature, 383, 45
Peletier, R. F. 1989, Ph.D. thesis, Groningen Univ.
Persson, S. E., Cohen, J. G., Matthews, K., Frogel, J. A., & Aaronson, M. 1983, ApJ, 266, 105
Quinn, P. J. 1984, ApJ, 279, 596
Renzini, A. 1977, in Advanced Stages of Stellar Evolution, ed. P. Bouvier & A. Maeder (Sauverny: Obs. Genève), 149
Rose, J. A. 1985, AJ, 90, 1927
Sandage, A., & Tammann, G. A. 1981, A Revised Shapley-Ames Catalog of Bright Galaxies (Washington: Carnegie Inst. Washington)
Schombert, J. M., & Wallin, J. E. 1987, AJ, 94, 300
Schweizer, F. 1978, in Structure and Properties of Nearby Galaxies, ed. E. M. Berlchuij & R. Wielebinski (Dordrecht: Reidel), 279
Schweizer, F. 1996, AJ, 111, 109
Schweizer, F., & Seitzer, P. 1992, AJ, 104, 1039 (SS92)
Schweizer, F., Seitzer, P., Faber, S. M., Burstein, D., Dalle Ore, C. M., & Gonzalez, J. J. 1990, ApJ, 364, L33
Silva, D. R., & Bothun, G. D. 1998, AJ, in preparation (Paper II)
Silva, D. R., & Elston, R. 1994, ApJ, 428, 511
Silva, D. R., & Wise, M. W. 1996, ApJ, 457, L15
Singh, K. D., Prabha, T. P., Kembhavi, A. K., & Bhat, P. N. 1994, ApJ, 424, 638
Smith, D. A., et al. 1996, ApJ, 473, L21
Tiede, G. P., Frogel, J. A., & Terndrup, D. M. 1995, AJ, 110, 2788
VandenBerg, D. A. 1988, in The Harlow Shapley Symposium on Globular Cluster Systems in Galaxies, ed. J. E. Grindley & A. G. Davis Philip (Dordrecht: Kluwer), 107
van den Bergh, S. 1981, A&AS, 46, 79
van Dokkum, P. G., & Franx, M. 1995, AJ, 110, 2027
Vassiladis, E., & Wood, P. R. 1993, ApJ, 413, 641
Wise, M. W., & Silva, D. R. 1996, ApJ, 461, 155
———. 1998, ApJ, submitted
Witt, A. N., Thronson, H. A., Jr., & Capuano, J. M., Jr. 1992, ApJ, 393, 611
Worthey, G. 1994, ApJS, 95, 107
Worthey, G., Faber, S. M., & González, J. J. 1992, ApJ, 398, 69